Available online at www.sciencedirect.com

ScienceDirect

Geochimica et Cosmochimica Acta 226 (2018) 224–243

Geochimica et Cosmochimica Acta

www.elsevier.com/locate/gca

Interplay of crystal fractionation, sulfide saturation and oxygen fugacity on the iron isotope composition of arc lavas: An example from the Marianas

H.M. Williams [a,*], J. Prytulak [b], J.D. Woodhead [c], K.A. Kelley [d], M. Brounce [e], T. Plank [f]

[a] Department of Earth Sciences, University of Cambridge, Downing Street, Cambridge, UK
[b] Department of Earth Science and Engineering, Imperial College London, UK
[c] School of Earth Sciences, The University of Melbourne, Parkville, VIC 3010, Australia
[d] Graduate School of Oceanography, University of Rhode Island, Narragansett, RI, USA
[e] The Department of Earth Sciences, The University of California Riverside, Riverside, CA, USA
[f] Department of Earth and Environmental Sciences, Columbia University, Lamont Doherty Earth Observatory, NY, USA

Received 2 October 2017; accepted in revised form 2 February 2018; Available online 13 February 2018

Abstract

Subduction zone systems are central to a multitude of processes from the evolution of the continental crust to the concentration of metals into economically viable deposits. The interplay between oxygen fugacity, sulfur saturation, fluid exsolution and fractionating mineral assemblages that gives rise to typical arc magma chemical signatures is, however, still poorly understood and novel geochemical approaches are required to make further progress. Here we examine a well-characterized suite of arc lavas from the Marianas (W. Pacific) for their stable Fe isotope composition. In agreement with previous work and mass balance considerations, contributions from sediments and/or fluids are shown to have negligible effect on Fe isotopes. Instead, we focus on disentangling processes occurring during basalt through dacite differentiation using a sample suite from the island of Anatahan. Anatahan whole rock Fe isotope compositions (δ^{57}Fe) range from -0.05 ± 0.05 to 0.17 ± 0.03 (2 S.D.)‰. A fractionation model is constructed, where three distinct stages of differentiation are required to satisfy the combined major and trace element and isotopic observations. In particular, the sequestration of isotopically heavy Fe into magnetite and isotopically light Fe into sulfide melts yields important constraints. The data require that lavas are first undersaturated with respect to crystalline or molten sulfide, followed by the crystallisation of magnetite, which then triggers late sulfide saturation. The model demonstrates that the final stage of removal of liquid or crystalline sulfide can effectively sequester Cu (and presumably other chalcophiles) and that late stage exsolution of magmatic fluids or brines may not be required to do this, although these processes are not mutually exclusive. Finally, the new Fe isotope data are combined with previous Tl-Mo-V stable isotope determinations on the same samples. Importantly, the multi-valent transition metal stable isotope systems of Fe and V are decoupled by sulfide saturation, thus providing a potential tool to constrain its somewhat intractable timing. The observed decoupling of notionally redox-sensitive tracers underlines the caution required in the application of transition metal isotopes as direct redox proxies.

Keywords: Subduction magmatism; Redox; Oxygen fugacity; Sulfur; Iron isotopes; Copper porphyry deposits

* Corresponding author.
E-mail address: hmw20@cam.ac.uk (H.M. Williams).

https://doi.org/10.1016/j.gca.2018.02.008
0016-7037/

1. INTRODUCTION

Oxygen fugacity (fO_2) is an intensive thermodynamic property that varies by several orders of magnitude in the solid Earth (Frost and McCammon, 2008). It is commonly expressed relative to equilibrium in the system fayalite-magnetite-quartz, based on relative abundance of ferric and ferrous iron (ΔFMQ; (Frost and McCammon, 2008)). Arc magmas typically have higher proportions of Fe^{3+} (and thus calculated oxygen fugacities) relative to mid-ocean ridge basalts (e.g., Carmichael, 1991, Arculus, 1994; Kelley and Cottrell, 2009; Brounce et al., 2014; Waters and Lange, 2016), coupled with high water (Kelley et al., 2010; Plank et al., 2013) and other volatile element contents (e.g. S, C, F) (Hedenquist and Lowenstern, 1994; Straub and Layne, 2003; Jenner et al., 2010). They are also characterized by higher contents of chalcophile (sulfur-loving) elements relative to MORB and are often spatially associated with Cu-Au-Ag ore deposits (e.g., Wilkinson, 2013).

The point at which magnetite appears on the liquidus during differentiation classically determines whether basaltic magmas follow calc-alkaline (Fe-depleted, early appearance of magnetite) or tholeiitic (Fe-enriched, late appearance of magnetite) trends (Osborn, 1959; Hamilton et al., 1964; Sisson and Grove, 1993; Toplis and Carroll, 1996). Efforts have been made to discriminate between calc-alkaline and tholeiitic trends by quantifying Fe enrichment and the role of water during differentiation with the introduction of the so-called 'tholeiitic index' (Zimmer et al., 2010). The appearance of oxide phases on the basalt liquidus is promoted by high melt $Fe^{3+}/\Sigma Fe$ (Osborn, 1959; Botcharnikov et al., 2008) which is generally correlated with high magmatic H_2O contents (Kelley and Cottrell, 2009; Zimmer et al., 2010), and in a closed system, early and extensive magnetite fractionation will serve to decrease melt FeO_{tot}, $Fe^{3+}/\Sigma Fe$ and apparent fO_2 (Brounce et al., 2014). This process will also change the SO_4^{2-}/S^{2-} of the melt, as dissolved SO_4^{2-} within the melt is reduced to S^{2-}, triggering sulfide saturation (Mavrogenes and O'Neill, 1999; Jenner et al., 2010; Jugo et al., 2010). The timing of sulfide saturation is critical in determining the chalcophile element contents of melts, and thus their potential to concentrate economically viable minerals, as in copper porphyry deposits (Sun et al., 2015). In tholeiitic systems, sulfide appears early on the liquidus (Mavrogenes and O'Neill, 1999; O'Neill and Mavrogenes, 2002) and rapidly depletes the melt in chalcophile elements. Conversely, the high oxygen fugacities recorded by arc lavas imply elevated SO_4^{2-}/S^{2-} ratios (e.g., Jugo et al., 2010) and may suppress the appearance of sulfide as a liquidus phase, which may allow the concentrations of chalcophile elements to increase in arc magmas during differentiation and fractional crystallization. A substantial decrease in the fO_2 of arc magmas, by the fractional crystallization of magnetite or by the degassing of oxidized sulfur species (Kelley and Cottrell, 2012), is required to decrease the $Fe^{3+}/\Sigma Fe$ and SO_4^{2-}/S^{2-} ratios of arc magmas, promoting the late appearance of sulfides that are highly concentrated in chalcophile elements on the liquidus.

The processes responsible for generating the apparently oxidized nature of arc lavas, coupled with their variable chalcophile and volatile element abundances, remain poorly understood. This in part stems from the complex nature of magmatic differentiation and degassing processes. In addition, the prior melt extraction history of the sub-arc mantle and possible contributions of sediment melt and slab fluid components to the mantle wedge add further ambiguity. Stable iron isotopes may offer a new means of disentangling these processes and contributions during magmatic differentiation.

1.1. Iron isotope variations in magmatic systems

The behavior of iron isotopes is generally well understood amongst non-traditional stable isotope systems in silicate materials (i.e. those other than C-H-O-N-S, see review in Dauphas et al., 2017). Isotope variations are reported here as $\delta^{57}Fe$, the per mil deviation in measured $^{57}Fe/^{54}Fe$ relative to the IRMM-014 Fe standard; with $\delta^{57}Fe \sim 1.5 * \delta^{56}Fe$. Theoretical calculations suggest that equilibrium Fe isotope fractionation will be driven by contrasts in Fe oxidation and coordination state (Polyakov and Mineev, 2000; Shahar et al., 2008; Young et al., 2015). During melt extraction and fractional crystallization processes, it is generally assumed that Fe^{3+} behaves more incompatibly than Fe^{2+} (Woodland and Koch, 2003). Thus, isotopically heavy Fe (i.e. ^{57}Fe and ^{56}Fe versus ^{54}Fe) is predicted to be concentrated in Fe^{3+}-bearing sites (such as those in present in magnetite and silicate melt structures) relative to Fe^{2+} (such as those in olivine, pyroxene, crystalline sulfide and sulfide melt structures) (Polyakov and Mineev, 2000; Shahar et al., 2008; Schuessler et al., 2009; Macris et al., 2015; Young et al., 2015; Sossi et al., 2016). In agreement with these predictions, recent studies employing Nuclear Resonant Inelastic Scattering (NRIXS) have observed that silicate melts do indeed have bond structures favouring the concentration of isotopically heavy Fe; this effect broadly correlates with melt $Fe^{3+}/\Sigma Fe$ such that melts with the highest ferric iron contents should have the heaviest Fe isotope compositions (Dauphas et al., 2014; Roskosz et al., 2015). As a tracer, Fe stable isotopes have the advantage that they only record the physical removal or addition of Fe under different conditions and, providing a closed system is retained, are insensitive to redox processes involving other elements (e.g. C, S). Furthermore, due to the large amounts of Fe required to perturb the Fe isotope compositions of mantle rocks, the Fe isotope compositions of igneous rocks should be relatively insensitive to the addition of fluid and sedimentary components.

Given the observations described above, MORB, OIB and arc lavas should have heavier $\delta^{57}Fe$ than their mantle source regions, if partial melting of their peridotitic and/or pyroxenitic mantle sources are the dominant control on their $\delta^{57}Fe$ compositions. This is observed in the case of MORB and OIB, which have mean $\delta^{57}Fe$ values in the order of ~0.1 to 0.2‰ heavier than fertile mantle peridotites (Weyer et al., 2005; Williams et al., 2005; Weyer and Ionov, 2007; Teng et al., 2013; Williams and Bizimis, 2014; Sossi et al., 2016), as well as the inferred $\delta^{57}Fe$ of

the primitive upper mantle (Dauphas et al., 2009). In contrast, arc lavas have lighter δ^{57}Fe values than those measured in MORB and OIB (Dauphas et al., 2009; Nebel et al., 2013, 2015). Extremely light (~−0.5‰) δ^{57}Fe values have also been reported for bulk samples and mineral separates from sub-arc mantle xenoliths from Kohistan and Simcoe (Williams et al., 2004, 2005). These light Fe isotope compostions were interpreted in terms of the concomitant oxidation and melt extraction from the mantle wedge following the infiltration of the suprasubduction zone mantle by slab derived fluids and removal of isotopically heavy Fe during partial melt extraction. A similar scenario was proposed to explain the light δ^{57}Fe of Banda arc basalts, although in that model, the depletion of the mantle wedge by melt extraction in the fore-arc is decoupled from later oxidation by slab-derived melts or fluids (Nebel et al., 2015).

Magmatic differentiation processes play a critical role in determining the Fe isotope compositions of igneous rocks. Three previous studies (Teng et al., 2008; Schuessler et al., 2009; Sossi et al., 2012) have specifically investigated the role of magmatic differentiation, demonstrating resolvable Fe isotope variations at high temperatures. In particular, Sossi et al. (2012) undertook a study on rocks and pyroxene-magnetite pairs from the tholeiitic Red Hill sill (Tasmania, Australia). In this suite, closed-system fractionation of pyroxenes and plagioclase gives rise to an iron enrichment trend and an increase in melt fO_2 and δ^{57}Fe, until the point at which magnetite appears on the liquidus, after which melt δ^{57}Fe, decreases, due to the removal of isotopically heavy Fe hosted in magnetite. Schuessler et al. (2009) performed a systematic Fe isotope study of genetically related basaltic to rhyolitic lavas from Hekla, Iceland. They found that melt δ^{57}Fe increased substantially, by ca 0.22‰, during melt evolution from dacitic to rhyolitic compositions, which they interpreted in terms of fractionation of isotopically light titanomagnetite from the melt. Comparison of the Schuessler et al. (2009) and Sossi et al. (2012) studies thus illustrates the importance of oxide composition and Fe oxidation on Fe isotope fractionation, with Fe^{3+}-rich magnetite ($Fe^{2+}Fe^{3+}_2O_4$) concentrating isotopically heavy Fe in contrast to the more Fe^{2+}-rich ulvöspinel ($TiFe^{2+}_2O_4$).

The contrasting trends in Fe isotope evolution observed in the Red Hills suite versus the Hekla suite have been interpreted in terms of differentiation in systems that are closed and open to oxygen exchange, respectively. In the Red Hills suite, clinopyroxene and plagioclase fractionation causes melt $Fe^{3+}/\Sigma Fe$ to increase up to the point of magnetite saturation, whereas Hekla melts evolve along a trajectory roughly equivalent to an fO_2 lying on the fayalite-magnetite-quartz buffer. The oxide phase (presumed to be magnetite) crystallising in the Red Hills suite has a high Fe^{3+} content and a composition approaching pure magnetite whereas in Hekla the lower melt Fe^{3+} results in the crystallization of titanomagnetite with higher ülvospinel content. The latter has a lower Fe^{3+} content and consequently does not display the same degree of preference for heavy δ^{57}Fe, such that magnetite crystallization in the Hekla suite does not result in the same dramatic fall in δ^{57}Fe as seen in Red Hills.

These studies demonstrate that Fe isotopes, in conjunction with other tracers, can provide a means of exploring the complex relationships between melt $Fe^{3+}/\Sigma Fe$ and magmatic differentiation processes. Although both olivine-pyroxene fractionation and magnetite saturation (for samples with <4 wt% MgO) have been invoked to explain broad variations in the Fe isotope compositions of Banda arc magmas (Nebel et al., 2015) there are no detailed studies of melt Fe isotope evolution in genetically related arc magmas or water-rich systems.

In this paper, we explore processes that may explain the variability and generally lighter Fe isotope composition of arc lavas compared with MORB and OIB. First, we address potential source variability and subduction inputs with new Fe isotope data for well-characterized arc lavas from six subaerial volcanic centers along the Central Island Province (CIP) of the Mariana arc (Anatahan, Guguan, Alamagan, Pagan, Agrigan, and Uracas). These volcanic centers have contrasting inputs of slab-derived sediment and fluid components to their mantle source regions (Elliott et al., 1997; Avanzinelli et al., 2012). Secondly, we focus on the island of Anatahan in the Marianas and its single volcano, which has erupted a range of differentiated products. We use the Anatahan suite to evaluate the effect of magmatic differentiation processes on the distribution of iron and sulfur in primitive to evolved arc magmas. Finally, we take advantage of the fact that the same sample powders analysed in this study have also been analysed for other heavy stable isotope systems including thallium (Tl), molybdenum (Mo) and vanadium (V) to examine variability in multiple stable isotope space and explore insights gained from combining stable isotope systematics.

2. SAMPLES AND GEOLOGICAL SETTING

The Mariana intra-oceanic volcanic arc results from the westward subduction of the Jurassic-aged Pacific Plate beneath the Philippine Plate (Fig. 1) and forms part of the ~2500 km long Izu-Bonin-Mariana (IBM) subduction zone. The mantle beneath the Marianas arc is thought to be more chemically depleted than MORB source mantle, a feature which has been ascribed to prior melting events beneath the back arc (Woodhead et al., 1993). The islands from the Mariana Central Island Province (CIP, Fig. 1) are characterized by abundant, intermediate to mafic Holocene eruptions that have been the focus of numerous previous studies (Meijer and Reagan, 1981; Woodhead and Fraser, 1985; Bloomer et al., 1989; Woodhead, 1989; Woodhead et al., 1993; Elliott et al., 1997; Shaw et al., 2008; Wade et al., 2008; Kelley et al., 2010; Avanzinelli et al., 2012; Martindale et al., 2013; Prytulak et al., 2013, 2017a, b; Freymuth et al., 2015). Magma compositions span the calc-alkaline to tholeiitic divide, and appear to be oxidized, based on the high $Fe^{3+}/\Sigma Fe$ ratios observed in olivine-hosted melt inclusions that have similar MgO contents to MORB (Kelley and Cottrell, 2009; Kelley et al., 2010; Brounce et al., 2014).

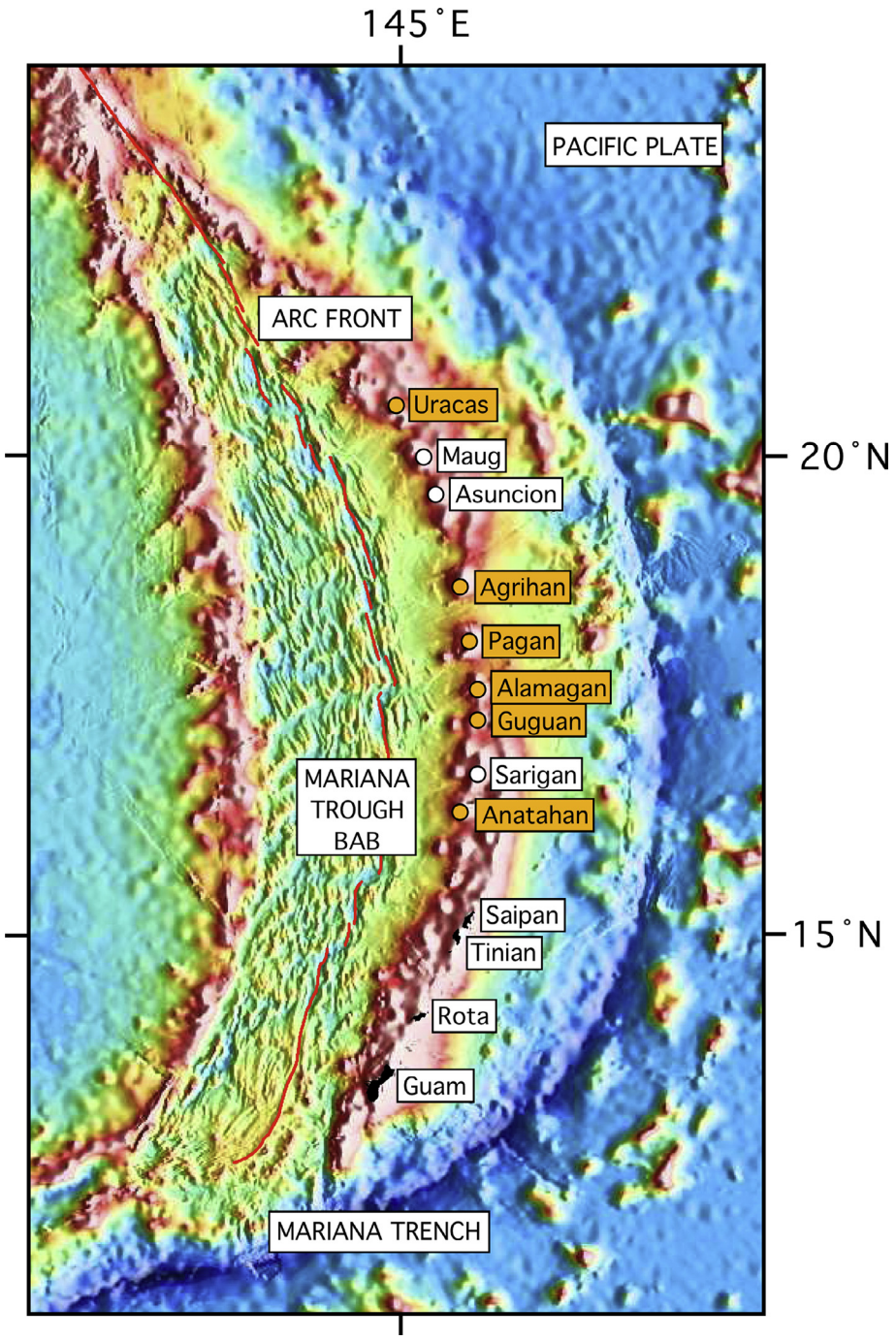

Fig. 1. Bathymetric map of the Mariana convergent margin in the Western Pacific, including Mariana Trench, Mariana Arc, and Mariana Trough backarc basin. This map was compiled from available bathymetric data by Fernando Martinez (U Hawaii) including decimated 1-min grid for Mariana Trough (Kitada et al., 2006). Swath-mapped bathymetry is recompiled and matched to predicted bathymetry from Sandwell and Smith (1997). Red line depicts the backarc basin spreading axis from Martinez and Taylor (2003). (For interpretation of the references to colour in this figure legend, the reader is referred to the web version of this article.)

The CIP samples studied here were originally sampled for U-series determinations, thus they are biased towards the most mafic and youngest material from each volcano. Prior studies have converged on the notion of distinct contributions to the petrogenesis of these lavas, including (1) an aqueous fluid derived from the altered mafic oceanic crust and (2) melts, largely derived from the subducting pelagic sediment pile (Elliott et al., 1997; Kent and Elliott, 2002; Avanzinelli et al., 2012; Prytulak et al., 2013; Freymuth et al., 2015). In broad terms, the aqueous "fluid" (i.e., H_2O-rich) component in the Marianas is characterized by low $^{87}Sr/^{86}Sr$ and high Pb/Ce, U/Th and

Ba/La relative to MORB, whereas the "sediment melt" (i.e., silicate liquid/melt) component is typified by negative Ce anomalies, unradiogenic $^{143}Nd/^{144}Nd$ and high Th/La.

Anatahan volcano erupts generally more evolved products relative to those from the other CIP islands and it provides a range of eruptive products from basaltic to dacitic compositions (Stern and Ito, 1983; Woodhead, 1989; Woodhead et al., 2001; Wade et al., 2005) derived from an isotopically homogeneous mantle source, thus providing an excellent opportunity to study the effect of magmatic differentiation processes on Fe stable isotopes in an arc setting.

We have analysed 16 samples from different CIP volcanic centers (Woodhead, 1989; Elliott et al., 1997; Wade et al., 2005) as well as 11 samples from Anatahan (Woodhead and Fraser, 1985; Woodhead, 1989; Woodhead et al., 1993, 2001; Wade et al., 2005). Below, we discuss the salient features of these volcanic centers and the specific samples analysed here. Plots of selected major and trace element concentrations versus MgO for the different CIP suites are presented in Fig. 2.

2.1. Sample descriptions

2.1.1. Agrigan

Agrigan lavas are basalts and basaltic andesites (Fig. 2) with trace element and isotopic signatures indicative of a sediment contribution to their mantle source region (e.g. high Th/La) (Stern and Ito, 1983; Woodhead, 1988, 1989; Elliott et al., 1997; Kent and Elliott, 2002; Plank, 2005). Olivine-hosted melt inclusions from Agrigan have high concentrations of dissolved H_2O (~5 wt%; (Shaw et al., 2008; Kelley et al., 2010)) and high $Fe^{3+}/\Sigma Fe$ ratios (up to 0.34; (Brounce et al., 2014)). Two samples from Agrigan were analysed here: a phyric basaltic andesite, MM-92-6 (Elliott et al., 1997) and a powdered tephra sample that contains phenocrysts of olivine, plagioclase, clinopyroxene, and magnetite (AGR19-02), which was previously studied by Kelley and Cottrell (2012). We also analysed clinopyroxene and magnetite mineral separates from the latter sample in order to explore the effects of degassing and late stage magmatic evolution processes on the distribution of Fe isotopes between these phases.

2.1.2. Alamagan

Alamagan samples are not particularly distinctive in terms of their major and trace element geochemistry relative to other CIP islands (Fig. 2), and display intermediate characteristics in terms of fluid (e.g. high Ba/La) and sediment (high Th/Nb) indices. They diverge from the main U-series trends evident in other CIP lavas, having both the highest $(^{230}Th/^{232}Th)i$ and lowest $(^{231}Pa/^{235}U)i$ ratios relative to other CIP samples (Elliott et al., 1997; Avanzinelli et al., 2012). Melt inclusions from Alamagan display ranges in S, CO_2 and H_2O concentrations that are consistent with sulfur and CO_2 degassing (Dixon et al., 1995; Brounce et al., 2014) and $Fe^{3+}/\Sigma Fe$ ratios that range from 0.207 to 0.267 and decrease with MgO content (Brounce et al., 2014). Two basaltic andesites from Alamagan (Alam 2, Alam 5) sampled by Elliott et al. (1997) were analysed here.

2.1.3. Guguan

Guguan lavas range from basalt to basaltic andesite and are characterized by low Th/La, Nb and REE contents relative to other CIP islands. Bulk samples also display a wide range in Cu contents, which show a broad positive correlation with MgO (Fig. 2f). Both bulk samples (Elliott et al., 1997) and olivine-hosted melt inclusions (Kent and Elliott, 2002; Kelley and Cottrell, 2009) display high Ba/La ratios consistent with the presence of aqueous slab fluid components in their mantle source regions. Olivine-hosted melt inclusions from Guguan display high $Fe^{3+}/\Sigma Fe$ ratios that are positively correlated with their water contents (Brounce et al., 2014). These data provide evidence in support of the oxidation of subarc mantle by hydrous slab fluids and the generation of primitive, oxidized arc magmas. We analysed the basalt/basaltic andesite flows GUG-9, GUG-11, GUG-12 and GUG-13 from the collection of Elliott et al. (1997) as well as two olivine bearing tephra samples from separate eruptions (samples 04-Gug-11 and Gug-23-02) which were collected by the MARGINS-NSF field expedition to the Mariana arc in 2004.

2.1.4. Pagan

Three moderately potassic basalts (PAG 1–3) from the Elliott et al. (1997) collection were analysed here. These samples are phyric lava flows and have major and trace element characteristics similar to other Pagan samples (NHNH 108982-5, 6, 8) previously analysed by Dauphas et al. (2009) for their Fe isotope compositions (Fig. 2). Taken together, the Pagan lavas display intermediate Ba/La and Th/Nb ratios relative to the other CIP samples. The single melt inclusion studied from a Pagan tephra has a $Fe^{3+}/\Sigma Fe$ ratio of 0.22, which is significantly higher than that of MORB at an equivalent MgO content (~7 wt%) (Brounce et al., 2014).

2.1.5. Uracas

We have analysed two basaltic andesites and an andesite from Uracas (URA 6, 7 and 12) that were collected by Elliott et al. (1997). These more evolved samples display many of the same geochemical features as Agrigan, i.e.) high Th/La, negative Nb anomalies on primitive-mantle normalized incompatible element diagrams and low ($^{238}U/^{230}Th$). As a consequence of their more evolved nature, samples from Uracas display notably lower concentrations of compatible elements (e.g. V, Cr; Fig. 2b and d).

2.1.6. Anatahan

Anatahan erupts a range of compositions from basaltic to dacitic and lavas span a range of MgO contents (Fig. 2). The lavas are commonly phyric, with phenocrysts including plagioclase, clinopyroxene and titaniferous magnetite, where the latter has been described as a solid solution of 62–66% magnetite ($Fe^{2+}Fe^{3+}_2O_4$) and 34–38% ulvospinel ($TiFe^{2+}_2O_4$) (de Moor et al., 2005). The evolved lavas on Anatahan originate by fractional crystallisation rather than other processes such as crustal assimilation (Wade et al., 2005), as evident in their tightly restricted radiogenic Sr-Nd-Pb isotope composition across the range of major element composition. Mafic samples are moderately potassic

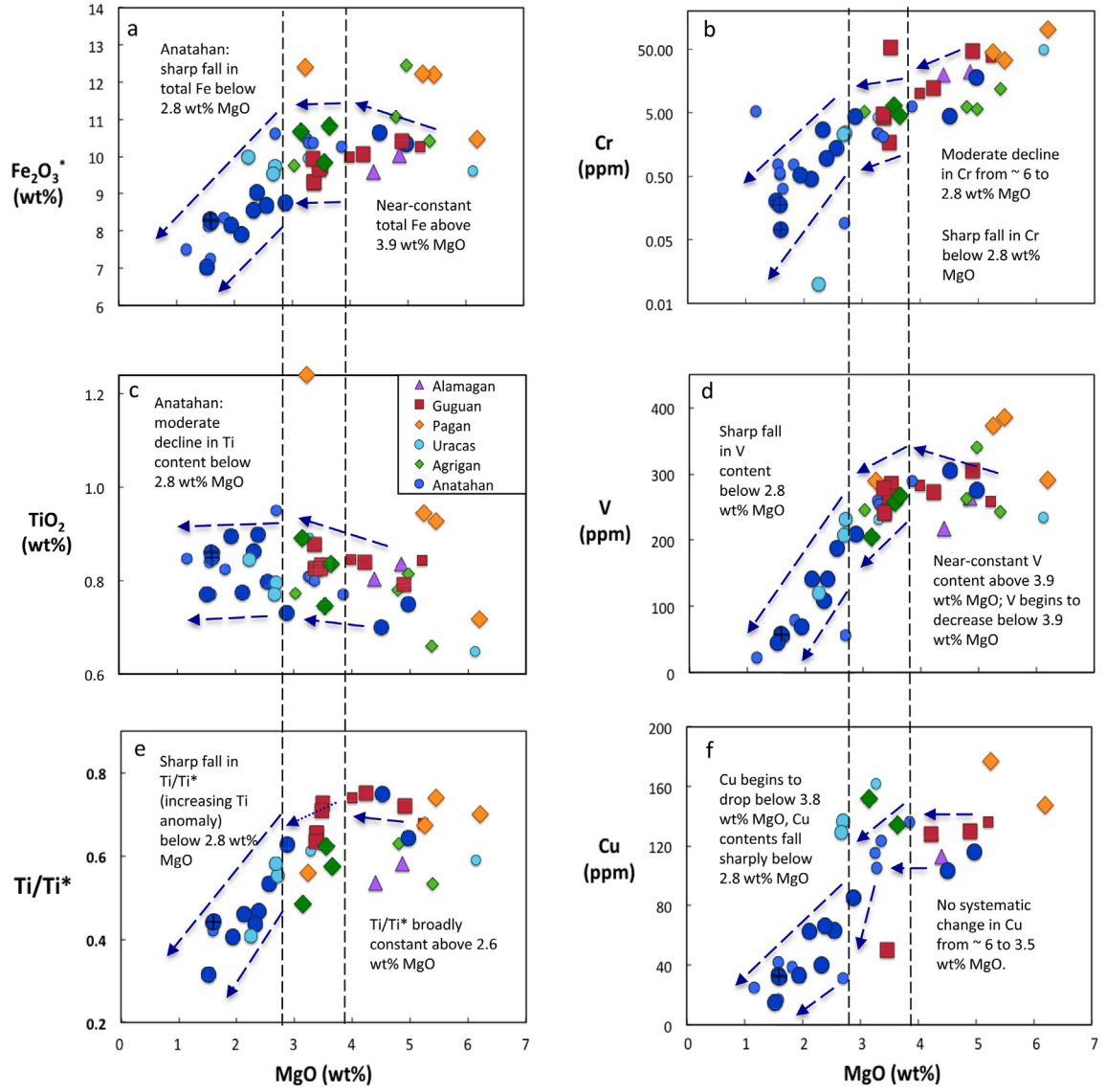

Fig. 2. Harker diagrams for major and trace elements in Anatahan and other CIP islands. Ti/Ti* refers to primitive-mantle (Palme and O'Neill, 2004) normalized Ti anomaly calculated relative to Gd and Tb. Data references are provided in the main text. Large symbols denote samples analysed for Fe isotopes in this study, smaller symbols denote samples belonging to the same studies for which major and trace element data is available but which were not selected for isotope analysis. Errors are smaller than symbol size. The appearance of magnetite on the liquidus at ~3.5 wt% MgO is readily apparent in the change of slope on the $Fe_2O_3^*$ (total), V, Ti/Ti* and Cr (note log scale) plots. Vertical dashed lines show the main distinctions between pre- and post- magnetite-in groups at 3.9 wt% MgO and the point of major sulfide saturation <2.8 wt% MgO, heavy blue dashed lines illustrate the overall trends of element behavior with respect to MgO that are discussed in the main text. (For interpretation of the references to colour in this figure legend, the reader is referred to the web version of this article.)

and follow a trend that roughly parallels the tholeiitic/calc-alkaline divide. More evolved samples are characterized by low Ti/Ti* (i.e. large Ti anomalies on primitive-mantle normalized multi-element diagrams), low Fe_2O_{3tot}, V, Cu, and Cr concentrations relative to the more mafic (MgO > 4 wt %) samples (Fig. 2). Anatahan samples also display geochemical features consistent with enrichment of their mantle source by very minor (1–3 wt%) contribution of a slab-derived sediment melt component (e.g., high Th/La; Wade et al., 2005). Olivine-hosted melt inclusions (MgO ~ 3.5–4 wt%) have H_2O contents that are slightly lower (3.4 wt%; (Shaw et al., 2008) than those from other CIP volcanic centers that sample mantle domains dominated by slab fluid components (e.g., Guguan, 4.5 wt%; (Kelley and Cottrell, 2009; Kelley et al., 2010), and the same melt inclusions also display relatively constant S contents of ~1100 ppm.

We have analysed a number of pre-historic Anatahan samples collected by the MARGINS team in 2004: 04-Anat-01 (andesite scoria), 04-Anat-03 (basaltic andesite bomb), 04-Anat-04 (basaltic andesite scoria), Anat-26-01 and Anat-26-02 (andesite ashes/lapilli). We also include a subset of the pre-historic Anatahan samples (AN-1, 2, 5,

7, 8, 10, 11, 12D, 12F) ranging from basaltic to andesitic in composition and the focus of a large body of work by Woodhead and co-authors (Woodhead and Fraser, 1985; Woodhead, 1988; Woodhead et al., 1993, 2001).

3. METHODS

Iron isotope analyses were carried out on whole-rock powders and, in the case of AGR19-02, hand-picked mineral grains. In the case of the latter, individual sample aliquots consisted of 40–60 mineral grains between 120–200 μm in size, picked under ethanol using a binocular microscope avoiding crystals with obvious cracks, minor signs of external alteration and mineral or fluid inclusions and were subsequently cleaned in ultrapure 18.2 Ω water prior to dissolution.

Sample dissolution, iron purification and isotopic analyses were undertaken at Durham University using established procedures (Hibbert et al., 2012; Williams and Bizimis, 2014). Iron yields were quantitative and chemistry blanks were <0.5 ng Fe, and negligible compared to the quantities of sample Fe (>300 μg) processed. Isotopic analyses were performed on a multiple-collector inductively coupled plasma mass spectrometer (MC-ICPMS; Thermo Neptune) in dry plasma mode with an Apex sample introduction system. Sample solutions consisted of 0.9–1.5 ppm Fe (different concentrations were chosen on different days according to instrument sensitivity) in 0.1 M HNO_3, and instrumental mass bias was corrected for by sample–standard bracketing where the sample and standard Fe beam intensities (typically 35–40 V ^{56}Fe for a standard 10^{11} Ω resistor) were matched to within 5%. Mass dependence, reproducibility and accuracy were evaluated by analysis of an in-house "iron chloride" salt standard ($\delta^{57}Fe = -1.04 \pm 0.06‰$; $\delta^{56}Fe = -0.70 \pm 0.05‰$, 2 S.D., n = 57) previously analysed in other studies (Hibbert et al., 2012; Williams and Bizimis, 2014). This particular standard does not require column processing and hence provides evaluation of mass spectrometry conditions alone. The international rock standard BIR-1 (Icelandic basalt) was also analysed over the course of this work, providing values in excellent agreement with those of previous studies (Weyer et al., 2005; Dauphas et al., 2009; Hibbert et al., 2012; Williams and Bizimis, 2014): $\delta^{57}Fe = 0.08 \pm 0.06‰$; $\delta^{56}Fe = 0.06 \pm 0.04‰$, 2 S.D., n = 4, where n corresponds to the number of replicate analyses of a single solution processed through column chemistry, carried out during the same analytical sessions as the standards. The long-term reproducibility (±0.06‰) for $\delta^{57}Fe$ is used on sample error bars in Figs. 3, 5 and 6.

4. RESULTS

The $\delta^{57}Fe$ values of the CIP sample suite are presented in Table 1 and vary from -0.08 ± 0.07 to $0.29 \pm 0.01‰$ (2 S.D.), encompassing values both substantially lighter and heavier than the published range for MORB (Beard et al., 2003; Weyer and Ionov, 2007; Teng et al., 2013; Williams and Bizimis, 2014). The mean $\delta^{57}Fe$ of the CIP samples is $0.10 \pm 0.18‰$ (n = 26) whereas that of MORB is $0.16 \pm 0.08‰$ (n = 61; (Williams and Bizimis, 2014)) and they represent statistically distinguishable populations (Student's *t*-test, 99% c.i.). In detail, there are subtle variations in the $\delta^{57}Fe$ values of lavas from different CIP islands, as plotted against different indices of magmatic differentiation (e.g., Fe_2O_{3tot}, MgO; Fig. 3). The Fe isotope compositions of the Pagan and Agrigan samples analysed here overlap with data from Dauphas et al. (2009), who measured three basalts from Pagan ($\delta^{57}Fe$ 0.03 ± 0.04 to $0.04 \pm 0.04‰$) and one from Agrigan ($0.04 \pm 0.04‰$). Due to a lack of corresponding trace element data, these samples are only shown on the plots of $\delta^{57}Fe$ vs. SiO_2, Fe_2O_{3tot} and MgO (Fig. 3a–c, Pagan: pale orange diamonds; Agrigan, pale green diamond) as no further trace element data were provided for them.

Agrigan sample AGR19-02 has a whole-rock Fe isotope composition of $0.16 \pm 0.03‰$; and clinopyroxene and magnetite $\delta^{57}Fe$ values of 0.17 ± 0.01 and $0.24 \pm 0.08‰$, respectively. The heavier $\delta^{57}Fe$ value of magnetite relative to clinopyroxene is consistent with stable isotope theory (Polyakov et al., 2007; Polyakov, 2009) and experiments (Shahar et al., 2008). The Fe isotope compositions of clinopyroxene and magnetite separates from AGR19-02 overlap with the range documented for natural samples (Heimann et al., 2008; Sossi et al., 2012). However, it is not possible to verify the exact degree to which these minerals reached isotopic equilibrium.

5. DISCUSSION

5.1. Primary mantle source influences

One of the attractions of the Mariana Islands is the systematic variation in trace element, radiogenic and short-lived isotopes that have been related to distinct fluid and sediment components (Elliott et al., 1997). Despite these elemental systematics, there are no clear co-variations of $\delta^{57}Fe$ with any classic 'fluid' or 'sediment' tracers such as Ba/Th, La/Sm, or short-lived or radiogenic isotopes. This provides strong evidence that, unlike other stable isotope tracers such as Mo (Freymuth et al., 2015) and Tl (Prytulak et al., 2013), addition of fluids and/or sediments from the subducting slab does not have a discernable control on the $\delta^{57}Fe$ composition of arc lavas. This may be initially surprising, as residual slab serpentinites (Debret et al., 2016) have fractionated Fe isotope compositions consistent with the release of isotopically fractionated fluids with light $\delta^{57}Fe$ signatures. However this can be understood in the context of the mass balance given the low Fe contents estimated for these fluids (Debret et al., 2016) versus the substantial Fe content of the mantle wedge.

An alternative explanation must be sought to explain the observed $\delta^{57}Fe$ variability of Mariana arc magmas. It is first useful to compare the CIP samples with MgO > 4 wt % (i.e., mafic samples) to MORB. Mafic lavas and tephras yield a mean $\delta^{57}Fe$ of $0.07 \pm 0.18‰$ (2 S.D.; n = 6) and incorporating mafic CIP samples studied by Dauphas et al. (2009) gives a similar value of $0.06 \pm 0.14‰$ (2 S.D.; n = 14). Thus, the mean $\delta^{57}Fe$ of the CIP magmas appears to be slightly lighter than mean MORB ($\delta^{57}Fe = 0.16 \pm$

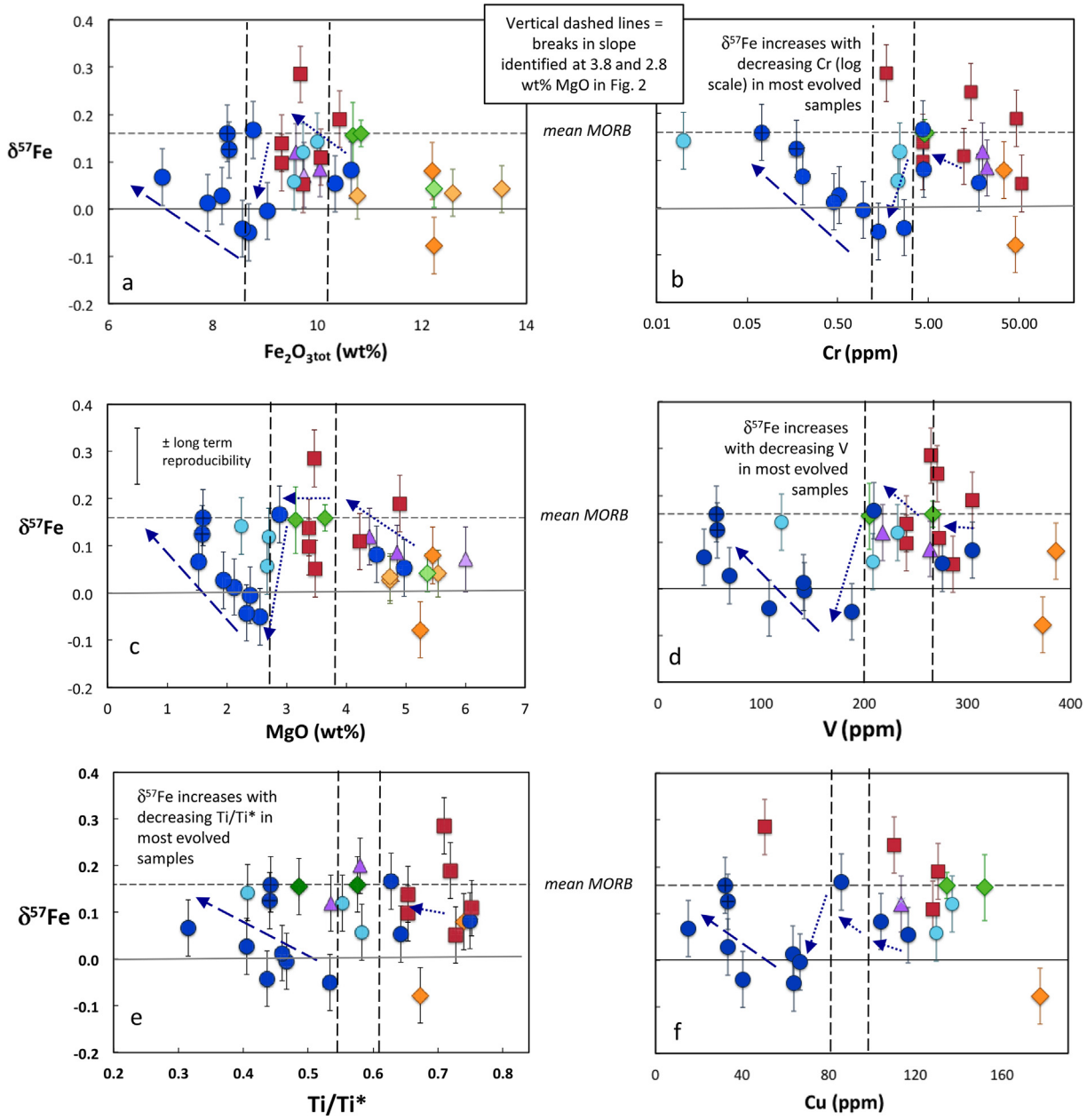

Fig. 3. Plots of bulk rock Fe isotope composition (δ^{57}Fe) versus major and trace element concentrations. Sample symbols are as in Fig. 2. Errors on Fe isotope composition are the 2 S.D. long term reproducibility, which is also shown as a bar for reference in panel (c). The horizontal dashed lines show the inferred Fe isotope composition of mean MORB (Teng et al., 2013; Williams and Bizimis, 2014). Most CIP samples cluster around a narrow range in δ^{57}Fe whereas the Anatahan suite displays a wider degree of variation. Vertical dashed lines correspond to 3.9 and 2.8 wt% MgO, as per Fig. 2, and are intended for reference, blue arrows illustrate the isotope trends discussed in the main text. (For interpretation of the references to colour in this figure legend, the reader is referred to the web version of this article.)

0.08‰ (n = 61; (Williams and Bizimis, 2014)), although there is substantial variation within the CIP. This broad difference of ~0.10‰ between CVZ and MORB δ^{57}Fe is in agreement with previous studies of arc basalts (Dauphas et al., 2009; Nebel et al., 2013, 2015) and mantle rocks (Williams et al., 2004, 2005). The lighter Fe isotope composition of arc rocks versus MORB was noted in these earlier studies and is consistent with the prediction that melt extraction leaves an isotopically light residue (Williams et al., 2005; Williams and Bizimis, 2014) and that certain arc lava source regions may be more depleted compared to MORB (Woodhead et al., 1993).

Mantle lithologic heterogeneity has also been proposed as a potential cause of Fe isotope fractionation (Williams and Bizimis, 2014). In particular, the presence of pyroxenite has been used to explain unusually heavy Fe isotope signa-

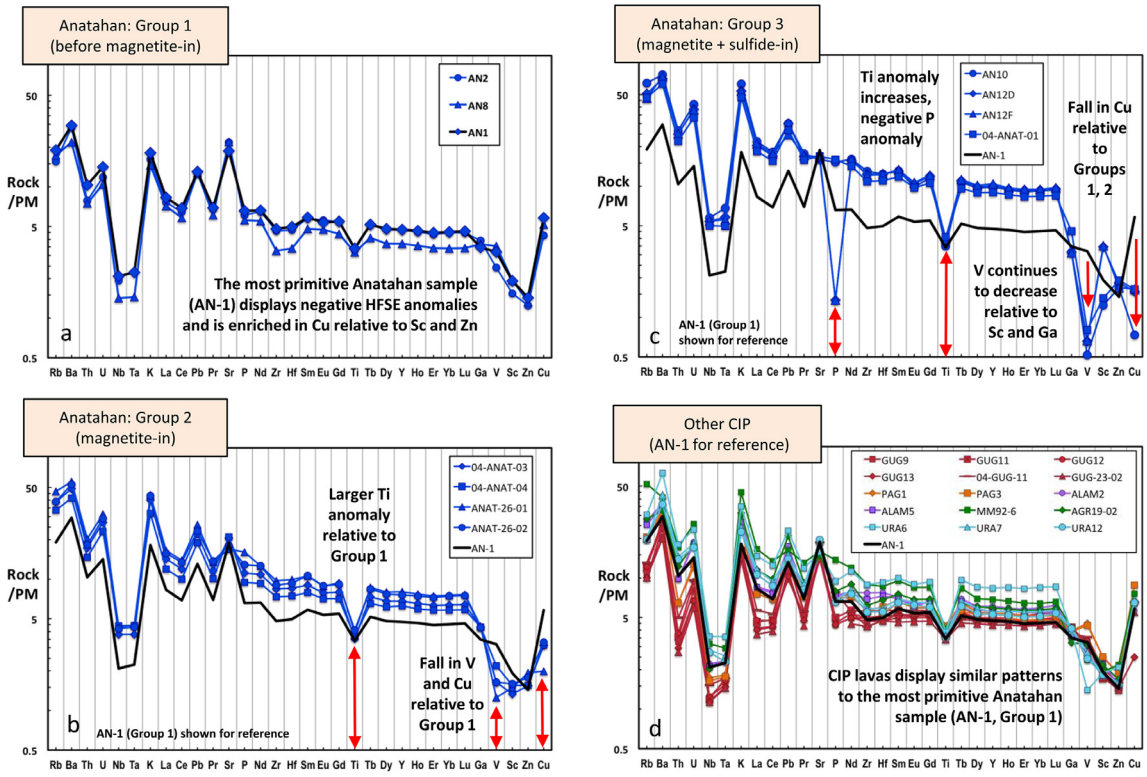

Fig. 4. Primitive mantle (Palme and O'Neill, 2004) normalized trace element diagram extended to transition elements. Element order modified after Jenner (2017). Anatahan samples have been divided into (1) a pre-(titano) magnetite saturation group; (2) a group recording the onset of magnetite (± minor sulfide) saturation and (3) a group recording extensive magnetite fractionation coupled with the inferred appearance of molten or crystalline sulfide on the liquidus. The pre-magnetite saturation Group 1 consists of samples that are comparatively primitive with high CaO, Fe_2O_{3tot} and MgO contents and characterized by the absence of negative V anomalies (relative to Ga and Sc), positive Sr and Pb anomalies and Cu contents that are strongly elevated relative to those of Zn, Sc, V and Ga and slightly elevated relative to Lu. The magnetite ± minor sulfide Group 2 displays a greater depletion of V relative to Ga and Sc, positive Sr and Pb anomalies and Cu contents that are elevated or similar to those of Zn but depleted relative to Ga and Lu. Group 3, which displays evidence for extensive magnetite and sulfide fractionation group is characterized by pronounced negative V anomalies and Cu contents that are depleted relative to Zn. (d) Other CIP samples. For the most part, these samples mirror the pattern of the Anatahan pre-magnetite saturation group in that they display positive Pb and Sr anomalies, an absence of negative V anomalies (with the exception of URA6, with displays a pronounced negative anomaly and the Pagan samples, which are characterized by positive V anomalies) and strong enrichment of Cu relative to Zn, Sc, V and Ga.

tures in ocean island basalts that are difficult to reconcile with melting and crystallisation processes alone (Williams and Bizimis, 2014; Konter et al., 2016). However, pyroxenite is a chemically enriched lithology and, if the variability was due to variable amounts of pyroxenite in the source, co-variations of Fe isotopes and trace element and/or radiogenic isotopes would be expected. Therefore, the Mariana lavas lack compelling evidence for a mantle source control on their Fe isotope compositions.

There are small differences in the degrees of magmatic differentiation of the CIP magmas, and it is possible that these differentiation processes dominate the variation in Fe isotope compositions observed. This is further investigated below, where we focus on the Anatahan suite of tephras, which display the maximum variability in their major and trace element compositions, and thus presumably are the most complete record of extensive magmatic differentiation of samples from this study (e.g., Wade et al., 2008).

5.2. Magmatic differentiation controls on Fe stable isotope compositions at Anatahan volcano

Sampled lavas from Anatahan volcano range in SiO_2 from 49.28 to 63.91 wt%, with little difference in radiogenic isotopes or evidence for crustal assimilation (Wade et al., 2005) and thus represent an ideal suite with which to investigate magmatic fractionation in an arc setting. The range in the extent of differentiation that is reflected in the composition of Anatahan samples can be illustrated using major and trace elements, in particular compatible V and Cr (Fig. 2d and g). The major and trace element plots in Fig. 2 show that most Anatahan samples have undergone extensive fractional crystallization, consistent with their petrography and eruption in an arc setting. Other islands, notably Guguan, Pagan and Agrigan span a narrower range of compositions. It is noteworthy that the less-evolved (>3.5 wt% MgO) Anatahan and CVZ lava samples have high Cu contents (>100 ppm; Fig. 2f)

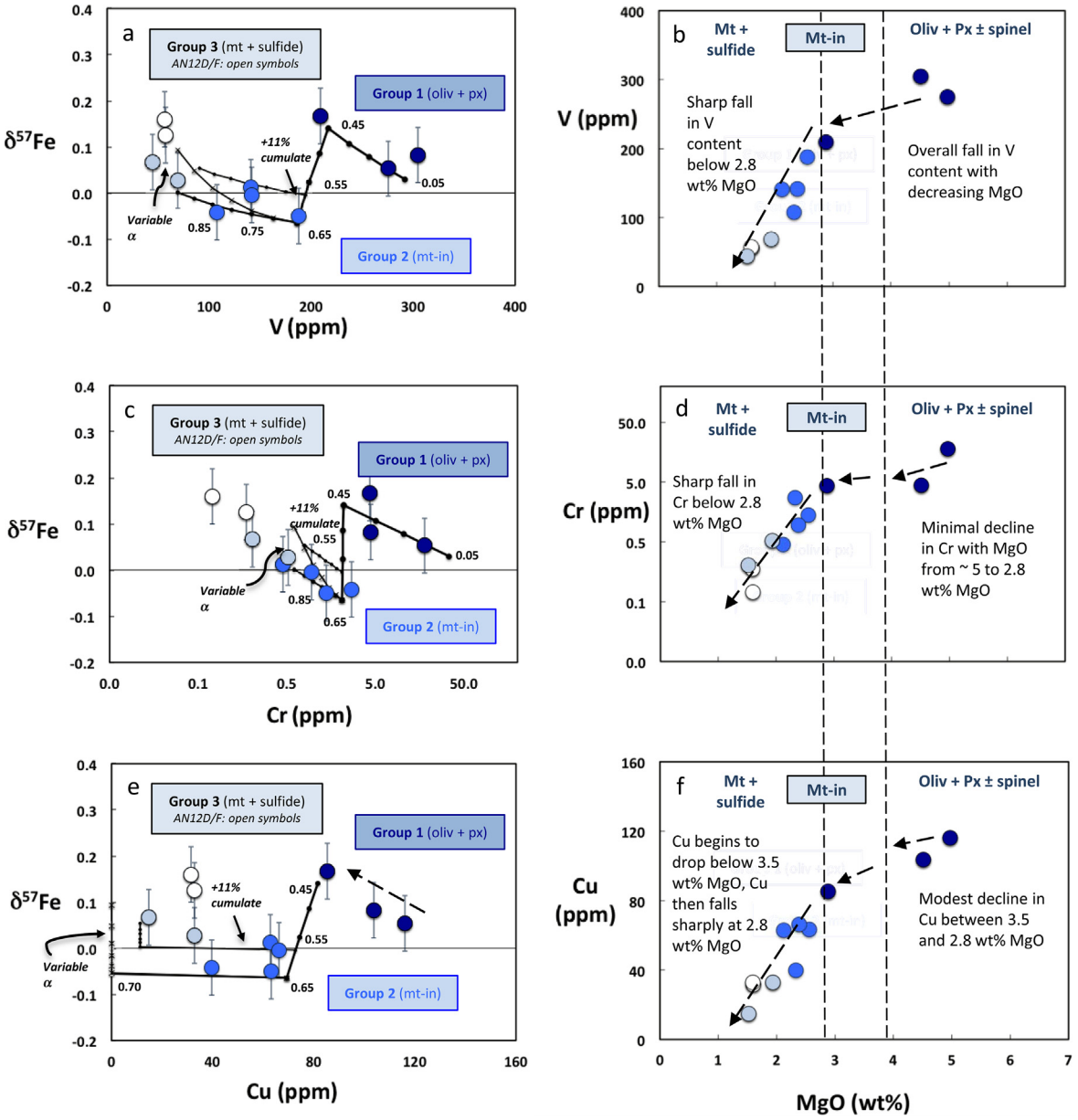

Fig. 5. Iron isotope compositions of Anatahan bulk samples plotted against V (a), Cr (c), Cu (e) with superimposed fractional crystallisation and mixing models (a–c), with corresponding plots of V (b), Cr (d), Cu (f) versus MgO for reference; arrows showing the main trends in element abundance with respect to Fe isotopes discussed in the text. It should be noted that only samples for which Fe isotope data are available are shown in panels b, d and f; for the full trace element versus MgO arrays refer to Fig. 2. The Anatahan suite has now been split into the groups used in Fig. 4. Pre-magnetite-saturated samples are dark blue, the onset magnetite samples medium blue and the extensive magnetite and sulfide fractionated samples pale blue, with the anomalous AN-12 samples denoted by open circles. In panels (a) and (b) the main curve displays a model of fractional crystallisation where the fractions of melt removed F (melt fraction removed) from 0.05 to 0.95 are shown increments of 0.05. Model details are in the main text. A mixing curve (89:11, labeled "+ 11% cumulate") between the sulfide-saturated part of the fractionation curve (F = 0.65 to F = 0.95) and the bulk cumulate formed from the magnetite saturation stage of the fractionation process is shown to illustrate the effects of incorporating small amounts of residual cumulate material. A modified model for the sulfide-saturated part of the fractionation curve (F = 0.65 to F = 0.95) is also shown (-x-). In this model, the melt-sulfide fractionation factor increases systematically with each increment of F. (For interpretation of the references to colour in this figure legend, the reader is referred to the web version of this article.)

relative to the Cu content inferred for primitive Mariana arc magmas (100–114 ppm (Jenner, 2017)). As Cu is highly compatible in sulfide (Gaetani and Grove, 1997; Ripley et al., 2002; Liu et al., 2014) the elevated Cu contents imply that significant sulfide saturation and segregation has not taken place at MgO contents >3.5 wt%, in contrast to MORB.

At Anatahan, the most dramatic changes in major and trace element behavior, evidenced by changes in slope on the element vs MgO plots, take place at ~3.5 wt% MgO.

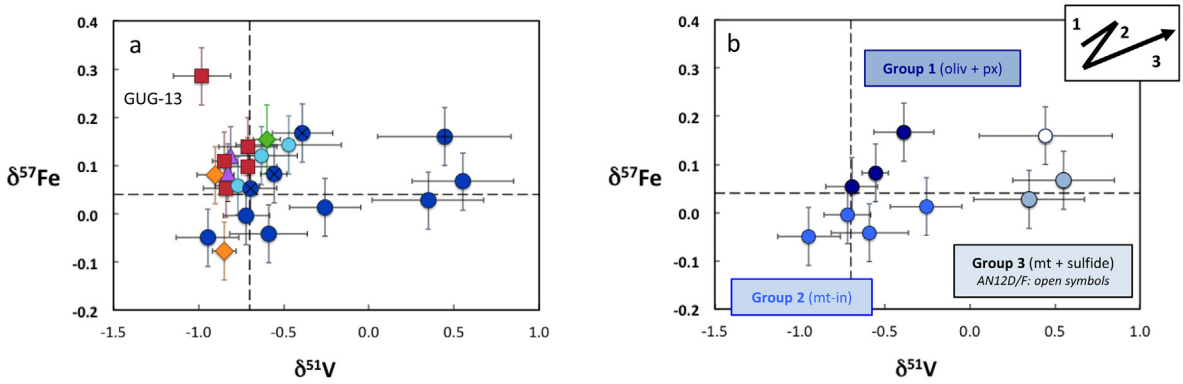

Fig. 6. Iron and vanadium isotope data for samples from the CVZ (a) and Anatahan differentiation suite (b). Symbols are as used in Fig. 2 (CIP) and Fig. 5 (Anatahan in panel b). A schematic curve showing the direction of the fractionation trend inferred for Anatahan is show as an inset on (b).

At this point, Fe_2O_3 (total), Ni, V, Cr, and Cu concentrations and Ti anomaly (Ti/Ti^*) (Fig. 2b–g) decrease sharply as MgO falls, consistent with fractionation of magnetite (Toplis and Corgne, 2002; Mallmann and O'Neill, 2009) and either crystalline or molten sulfide melt at MgO < 3.5 wt%. Extensive magnetite fractionation is evident in the presence of abundant oxide phenocrysts and inclusions in Anatahan samples although primary S-bearing phases are not observed (de Moor et al., 2005). As discussed by de Moor et al. (2005), the oxide phase crystallising can be described in terms of a titaniferous magnetite solid solution of magnetite and ulvospinel end-members in average proportions 66:34, respectively.

Anatahan lavas display two distinct shifts in $\delta^{57}Fe$ that appear to correlate with indices of magmatic differentiation (Fig. 3). The first of these is an abrupt fall in $\delta^{57}Fe$ between 3.5 and 2.8 wt% MgO (Fig. 3c); the second is a subsequent return to heavier $\delta^{57}Fe$ values below 2.8 wt% MgO. These shifts in $\delta^{57}Fe$ are most striking on the plots of Cr (Fig. 3b), V, (Fig. 3d) and Cu (Fig. 3f). As the contents of Cr and V decline from 17.9 to 4.3 ppm and 305 to 210 ppm, respectively, $\delta^{57}Fe$ appears to increase slightly (relative to the long-term reproducibility of ±0.06‰, a highly conservative estimate of uncertainty) from a value between 0.05 and 0.08‰ (samples AN-1, AN-8) to a maximum of 0.17‰ (AN-2). Between 4.3 and 1.4 ppm Cr and 210 and 188 ppm V, $\delta^{57}Fe$ drops rapidly from this maxima to a minima of −0.05 (sample 04-ANAT-04), after which $\delta^{57}Fe$ progressively increases with decreasing Cr and V. In the case of Cu, $\delta^{57}Fe$ initially increases as Cu contents decrease from ~120 ppm to ~80 ppm, below which they slowly return to heavier values (Fig. 3f). It should be noted that the highly evolved AN12 intrusive/lava lake samples (indicated with a "+") lie slightly off the arrays of $\delta^{57}Fe$ vs. V, Cr, Cu and Nb and these samples also display higher $\delta^{57}Fe$ values for given Fe_2O_3 and TiO_2 contents (Fig. 3a and c).

The relationships between $\delta^{57}Fe$ with major (Mg, Si, $Fe_2O_3^*$, Ti/Ti^*) and trace (V, Cr) elements in the Anatahan lavas are similar to those observed in the tholeiitic Red Hills suite (Sossi et al., 2012) and in Banda Arc samples (Nebel et al., 2015). The initial increase in $\delta^{57}Fe$ from MgO contents of 6.0–4.3 wt% is consistent with fractionation of isotopically light Fe^{2+}-bearing clinopyroxene and olivine (± plagioclase, although this phase will not affect Fe mass balance or $\delta^{57}Fe$), which will progressively increase both $\delta^{57}Fe$ and $Fe^{3+}/\Sigma Fe$ of the melt. High melt $Fe^{3+}/\Sigma Fe$ ratios are known to promote the appearance of magnetite on the liquidus (Hamilton et al., 1964; Sisson and Grove, 1993; Toplis and Carroll, 1995) and this is consistent with the sharp fall in $\delta^{57}Fe$ at ~2.8 wt% MgO, ~54 wt% SiO_2, ~5 ppm Cr and ~200 ppm V, as magnetite is known to concentrate these elements and isotopically heavy Fe (Polyakov and Mineev, 2000; Polyakov et al., 2007; Shahar et al., 2008; Sossi et al., 2012), the latter due to the large proportion of Fe^{3+} in its structure (in contrast to Fe^{2+}-bearing ulvöspinel; $TiFe_2^{2+}O_4$). The removal of significant amounts of magnetite from the melt by ~53 wt% SiO_2 is also consistent with the progressive decrease in the (primitive mantle normalized) abundance of V relative to Sc and Gd with increasing degree of differentiation (Fig. 4). In Fig. 4, the Anathan samples have been divided into three sequential groups: (1) pre-magnetite saturation; (2) magnetite saturated (possibly with the onset of sulfide-saturation); and (3) highly evolved, with extensive magnetite and sufide-saturated. Sulfide (either molten or crystalline) saturation in the more evolved Anatahan samples is evident in the pronounced decrease in Cu content relative to Zn and Ga (Fig. 4c) as Cu is known to be highly compatible in sulfide phases (Gaetani and Grove, 1997; Ripley et al., 2002; Liu et al., 2014). Sulfide saturation is also consistent with the steep decrease in bulk rock Cu content from 116 ppm at 4.9 wt% MgO (AN-1) to 14.7 ppm at 1.5 wt% MgO (AN-10) shown in Fig. 2f.

While the fractionation of significant amounts of magnetite can explain the abrupt *decrease* in melt $\delta^{57}Fe$ during differentiation due to the concentration of isotopically heavy Fe in this phase (Shahar et al., 2008; Sossi et al., 2012), another striking feature of the Anatahan differentiation sequence is the progressive *increase* in $\delta^{57}Fe$ as MgO decreases from 2.8 to 1.5 wt%, which is well outside the range of uncertainties on individual sample measurments or, even more conservatively, the long-term reproducibility on $\delta^{57}Fe$ (Fig. 3). Assimilation of mafic

Table 1
Mariana CIP Fe isotope compositions with selected major and trace element and V isotope data.

Sample	MgO (wt%)	Fe_2O_3* (wt%)	$\delta^{56}Fe$	2 S.D.	$\delta^{57}Fe$	2 S.D.	n	V (ppm)	Cr (ppm)	Cu (ppm)
Anatahan										
AN-8	4.51	10.65	0.03	0.05	0.08	0.07	4	305	4.42	104
AN-1	4.97	10.34	0.05	0.01	0.05	0.04	3	275	17.93	116
AN-2	2.88	8.77	0.09	0.08	0.17	0.03	3	210	4.32	85
04-Anat-04	2.56	8.69	−0.03	0.02	−0.05	0.05	5	188	1.39	63
Anat-26-02	2.39	9.04	0.00	0.04	0.00	0.08	4	142	0.96	66
04-Anat-03	2.12	7.90	0.03	0.04	0.01	0.07	5	141	0.45	63
Anat-26-01	2.33	8.57	−0.04	0.06	−0.04	0.08	4	108	2.72	40
04-Anat-01	1.94	8.16	0.04	0.03	0.03	0.05	4	69	0.52	33
AN-10	1.52	7.03	0.06	0.04	0.07	0.06	4	44	0.20	15
AN-12F	1.59	8.31	0.09	0.10	0.13	0.04	2	58	0.18	33
AN-12D§	1.60	8.27	0.09	0.06	0.16	0.08	1	57	0.07	32
Guguan										
GUG-9	4.23	10.07	0.06	0.04	0.11	0.05	5	272	12.30	128
GUG-11.4	3.38	9.32	0.11	0.02	0.14	0.08	2	241	4.30	–
GUG-11.5§	3.38	9.32	0.07	0.06	0.10	0.08	1	241	4.30	–
GUG-12	3.49	9.73	0.05	0.04	0.05	0.07	6	286	53.20	–
GUG-13	3.47	9.67	0.14	0.04	0.29	0.01	2	265	1.70	50
04-GUG-11	4.90	10.42	0.13	0.06	0.19	0.04	4	304	46.77	130
GUG-23-02			0.17	0.05	0.25	0.07	3	271	14.50	110
Alamagan										
ALAM-2	4.40	9.58	0.05	0.11	0.12	0.01	2	218	19.70	113
ALAM-5	4.86	10.05	0.13	0.06	0.20	0.08	2	264	22.10	–
Pagan										
PAG-1	5.45	12.19	0.00	0.00	0.08	0.00	2	386	33.71	
PAG-3	5.25	12.23	−0.04	0.02	−0.08	0.07	3	373	44.90	177
Agrigan										
MM-92-6	3.15	10.67	0.13	0.10	0.16	0.07	2	205	–	152
AGR19.02	3.65	10.83	0.07	0.04	0.16	0.03	2	266	4.52	134
AGR19.02 cpx			0.09	0.03	0.17	0.01	2	–	–	–
AGR19.02 mt§			0.14	0.06	0.24	0.08	1	–	–	–
Uracas										
URA-6	2.25	9.99	0.08	0.09	0.14	0.05	3	120	0.01	–
URA-7	2.71	9.73	0.06	0.09	0.12	0.06	5	232	2.40	137
URA-12	2.68	9.55	0.04	0.04	0.06	0.04	3	208	2.30	129

2SD errors calculated from replicate analyses of the sample solutions spread across different analytical sessions.
* Total Fe.
§ Where only one replicate was analysed, the long-term reproducibility was assigned as the sample error.

crust (or earlier erupted Anatahan lavas) with a $\delta^{57}Fe$ value equivalent to that of the isotopically heaviest evolved sample (~0.16‰) or even a magnetite-bearing cumulate from earlier stages of magmatic differentiation could potentially explain this increase. However, the assimilant would need to be Fe-rich and this would result in a positive correlation between $\delta^{57}Fe$ and Fe_2O_{3tot} in the most evolved samples. Such a correlation is not observed (Fig. 3c) and correlations between $\delta^{57}Fe$ and other indices of mafic crust assimilation such as oxygen isotopes are absent, consistent with previous studies that did not find evidence for crustal assimilation in Anatahan (Wade et al., 2005).

An alternative explanation for the progressive increase in $\delta^{57}Fe$ in the most evolved Anatahan samples could be fractionation and segregation of a Fe-rich but isotopically light phase. It has been suggested that the exsolution of aqueous, reduced, Fe^{2+}-bearing and isotopically light fluids could explain the heavy Fe isotope compositions of granitoids from a range of tectonic settings (e.g. Poitrasson and Freydier, 2005; Heimann et al., 2008). However, fluid exsolution at these low silica contents is unlikely, as the low degree of melt polymerization will promote water solubility in the melt (Schmidt et al., 1999). Moreover, such a fluid would need to be extremely enriched in Fe in order to change the Fe isotope compositions of the remaining silicate melt. Another phase that sequesters isotopically light Fe is required, and, as discussed below, either crystalline sulfide or sulfide melt is considered to be the most likely candidate.

5.3. Evidence for late sulfide saturation during differentiation of Anatahan magmas

Iron isotope fractionation experiments between silicate and pyrrhotite ($Fe_{1-x}S$) melts (Schuessler et al., 2007) have demonstrated that pyrrhotite accommodates isotopically light Fe relative to silicate phases. Sulfide saturation in arc magmas can be promoted by the appearance of magnetite on the liquidus, which, in a closed system serves to decrease melt $Fe^{3+}/\Sigma Fe$ and Fe_2O_{3tot} to the extent that dissolved sulfate in the melt is reduced to sulfide (Jenner et al., 2010).

The patterns defined by Anatahan samples on the primitive mantle-normalized multi-element diagrams (Fig. 4a–c) also provide evidence in support of late sulfide saturation triggered by magnetite fractionation. Prior to magnetite-in, relatively primitive, high MgO Anatahan samples display primitive mantle-normalized Cu contents that are elevated relative to the HREE, Ga, V, Sc and Zn (Fig. 4a, in which the order reflects compatibility during parental MORB genesis and is taken from Jenner, 2017). The appearance of magnetite on the liquidus at ~2.8 wt% MgO is apparent in Fig. 4b, where V abundance falls sharply relative to Ga to levels similar to Sc and Zn. Normalized Cu abundances are also lower relative to Ga and the HREE in these samples. This could reflect the partitioning of Cu into magnetite or clinopyroxene, or as Cu partitions most strongly into sulfides (Ripley et al., 2002; Liu et al., 2014), the onset of crystalline or liquid sulfide saturation. In the most evolved samples (Fig. 4c) significant fractionation of either crystalline or liquid sulfide phases is evident from the low abundance of Cu relative to Zn [Cu < Zn], Ga and the HREE. All of these samples display extremely low V abundances relative to Ga and Sc, implying that magnetite remains on the liquidus during this phase of differentiation. The anomalous samples Anat-12D and 12F display much more dramatic negative V anomalies with respect to Ga and Sc in Fig. 4c. These samples also display negative P anomalies indicative of apatite fractionation, in agreement with (Wade et al., 2005), who observed evidence for apatite saturation in evolved Anatahan melts. As Fe^{3+} promotes P solubility in melts (Mysen, 1992; Toplis et al., 1994; Jayasuriya et al., 2004) apatite saturation (and the implied decrease in melt P solubility) provides further evidence for a significant reduction in melt $Fe^{3+}/\Sigma Fe$ below 2.8 wt% MgO, consistent with extensive magnetite fractionation in Anatahan.

In Fig. 5, we have constructed a series of first-order crystal fractionation models using mass balance and Rayleigh isotope fractionation to illustrate the possible effects of magnetite fractionation and sulfide saturation on the evolution of Anatahan magma $\delta^{57}Fe$ with V, Cr and Cu (Fig. 5). Model D values were calculated from a compilation of published studies (Gaetani and Grove, 1997; Ripley et al., 2002; Mallmann and O'Neill, 2009; Liu et al., 2014). Bulk D values for Cr and V for the pre-, onset- and extensive magnetite fractionation groups were Cr: 5.84, 1.11, 2.99 and V: 1.32, 1.35, 2.60. The high value for Cr in the first stage of fractionation is due to the presence of minor Cr-spinel at this stage. Copper bulk D values for the latter two stages of the differentiation sequence are 1.38 and 112.3. For simplicity, only the Anatahan samples are shown and these have been divided into the same groups as used in Fig. 4a–c, with the anomalous AN-12 samples indicated by open circles. Corresponding Harker plots for V, Cr and Cu are also shown in Fig. 5.

In Fig. 5, $\delta^{57}Fe$ is plotted against V (a) and Cr (c), with the fractional crystallisation models superimposed. The models assume, for simplicity, that all Anatahan samples derive from a single starting composition of $\delta^{57}Fe$ = 0.02‰, V = 312 ppm and Cr = 44 ppm, based on the Fe isotope composition and trace element abundances of the most primitive Anatahan samples. Group 1 samples represent the first stage of fractionation (F = 0.01–0.45), where olivine (0.20, as a fraction of F), clinopyroxene (0.68) and Fe^{3+}-poor spinel (0.12) are assumed to be on the liquidus for F (melt fraction out) = 0.05–0.45. Group 2 samples correspond to F = 0.45–0.65. When magnetite appears on the liquidus, the fractionating assemblage consists of olivine (0.05), clinopyroxene (0.15), plagioclase (0.7343), trace sulfide (0.0007) and magnetite (0.065). In the final phase, represented by Group 3 samples, (F = 0.65–0.85) clinopyroxene (0.14), plagioclase (0.50), magnetite (0.08) and sulfide (0.28) are assumed to be on the liquidus. Feldspar is assumed to contain insignificant Fe to perturb Fe isotope mass balance. Mineral-melt fractionation factors were calculated by recasting inter-mineral fractionation factors relative to clinopyroxene ($\Delta^{57}Fe_{min\text{-}cpx}$), into $\Delta^{57}Fe_{melt\text{-}min}$ values, treating $\Delta^{57}Fe_{melt\text{-}cpx}$ as a free variable (Eq. (1)).

$$\Delta^{57}Fe_{melt\text{-}min} = \Delta^{57}Fe_{melt\text{-}cpx} - \Delta^{57}Fe_{min\text{-}cpx} \quad (1)$$

This approach was chosen at it allows $\Delta^{57}Fe_{min\text{-}cpx}$ values, which can be empirically constrained by studies of equilibrated natural samples, to be maintained. In the models below, an $\Delta^{57}Fe_{melt\text{-}cpx}$ value of 0.15‰ was used, based on the observed difference in mean Fe isotope composition between oceanic basalts and unmetasomatised fertile mantle peridotites (Williams and Bizimis, 2014). The values of $\Delta^{57}Fe_{min\text{-}cpx}$ used were: olivine (−0.20), spinel (−0.1), clinopyroxene (0), magnetite (0.8), sulfide (−0.45) and are based on experimental data (Schuessler et al., 2007; Shahar et al., 2008) and data for natural samples (Williams et al., 2005; Weyer and Ionov, 2007; Sossi et al., 2012). We have used a fractionation factor consistent with magnetite removal rather than ulvospinel removal as oxide compositional data (de Moor et al., 2005) indicate that the oxides present in Anatahan have a high (average 64%) end-member magnetite component. However, it should be noted that the value used in our models to fit the data array is greater than the observed difference in magnetite and clinopyroxene $\delta^{57}Fe$ values from the sample AGR19-02 as well as that predicted for Fe^{3+}-bearing spinels by Roskosz et al. (2015). This could suggest fractionation at lower temperatures or even the effects of isotopic diequilibrium. The resulting $\Delta^{57}Fe_{melt\text{-}min}$ were weighted according to mineral modal abundance and FeO^* content (olivine 17 wt%, clinopyroxene 10.9 wt%, spinel 6.5 wt%, magnetite 65 wt%, sulfide 69 wt%) to obtain a bulk melt-solid fractionation factor ($\Delta^{57}Fe_{melt\text{-}solid}$; Eq. (2)), which

was then used in standard Rayleigh fractionation equations. Mass balance (corrected for the amount of melt remaining) was conserved in all stages of the model.

$$\Delta^{57}Fe_{melt\text{-}solid} = \left(\sum_{i=1}^{n}[n_i \cdot \Delta^{57}Fe_{melt\text{-}min} \cdot FeO_{min}] \Big/ \sum_{i=1}^{n}[n_i \cdot FeO_{min}]\right) \quad (2)$$

The results of these calculations are shown in Fig. 5a and b. In order to illustrate the effects of variable $\Delta^{57}Fe_{melt\text{-}solid}$ on melt $\delta^{57}Fe$ a modified Rayleigh fractionation model was calculated for the final sulfide-saturated phase of differentiation where $\Delta^{57}Fe_{melt\text{-}solid}$ was decreased by 0.025‰ (in terms of α, 0.000025) at each increment of F = 0.05. This approach allows for a potential decrease in isotopic fractionation between melt and residue due to increased levels of Fe^{3+} in the melt following sulfide segregation and removal of $Fe^{2+}S$.

The fractionation models replicate the observed trajectories of $\delta^{57}Fe$ against Cr and V (Fig. 5a and c) reasonably well, and can replicate the abrupt drop in $\delta^{57}Fe$ at ~2.8 wt% MgO. This drop coincides with the appearance of magnetite on the liquidus, as evidenced by the sharp falls in melt Cr and V at this point (Fig. 5b and d) and is produced by the sequestration of isotopically heavy Fe into magnetite. Interestingly, melt Cr and V begins to decrease slightly earlier, between ~5 and 2.8 wt% MgO, which could reflect the partitioning of these elements into clinopyroxene and spinel before the onset of magnetite crystallization. The models also successfully reproduce the progressive increase in melt $\delta^{57}Fe$ below 2.8 wt% MgO, as this (in the context of the model) is produced by the removal of isotopically light Fe hosted in molten or crystalline sulfide. This is particularly successful when a variable $\Delta^{57}Fe_{melt\text{-}solid}$ is used in the final sulfide saturated differentiation stage, as discussed above. The model curves do not extend to the lowest Cr and V samples, including ANAT-12D and 12F, which were sampled from a different magmatic body. This may reflect the derivation of these samples from primary melts with subtly different $\delta^{57}Fe$ values, reflecting the fact they are not cogenetic with the other Anatahan samples.

Modeling the evolution of $\delta^{57}Fe$ against Cu (Fig. 5f) is challenging, in part because it is difficult to precisely determine the point where melt Cu contents begin to decrease (c.f. Fig. 2f, which shows that Anatahan melt Cu contents are high and scattered >3.5 wt% MgO, begin to decrease between 3.5 and 2.8 wt% MgO and decrease sharply at <2.8 wt% MgO). Before magnetite-in at 2.8 wt% MgO, fractionation of a melt with a Cu content approximating that inferred for primitive Mariana arc lavas (100–114 ppm; (Jenner, 2017)) and assuming fractionation of olivine + pyroxene + spinel ± plagioclase predicts melts with much higher Cu concentrations than those observed. This is function of the very low experimental D values for these phases (Liu et al., 2014). One possibility is that amphibole is on the liquidus at this stage, as it has been suggested that Cu is slightly compatible (average D~1.45) in this phase (Adam and Green, 2006) and a study of coexisting amphibole and pyroxene in an alkaline igneous rock suite (Schoenberg et al., 2009) suggests that amphibole could be expected to have a $\delta^{57}Fe$ value 0.15‰ lighter than clinopyroxene at ~700 °C. However, Cu is not sufficiently compatible to have a strong effect without major (~40 modal percent of the fractionating assemblage) amphibole removal and there is no petrographic or trace element evidence in support of extensive amphibole fractionation at Anatahan. Another possibility could be that the melts were buffered with respect to sulfide melt >2.8 wt%, which would allow for their relatively high and constant melt Cu contents (105–134 ppm) and relatively minor Fe isotope variations, which at this stage are controlled by olivine, pyroxene and spinel. In this scenario, sulfides would not segregate because they are in a cycle of being exsolved and resorbed by silicate melt. Extensive sulfide saturation and segregation, with its concomitant effects on melt $\delta^{57}Fe$ isotope composition only appears to take place later, at <2.8 wt% MgO, after magnetite-in. Therefore, the fractionation model shown in Fig. 5e only attempts to replicate the post magnetite-in stages (i.e. Groups 2 and 3) of differentiation, i.e. the rapid drop in $\delta^{57}Fe$ against Cu and the progressive return to isotopically heavier values with increasing differentiation. Although the model broadly achieves this, it can be seen in Fig. 5e that the calculated Cu contents of melts generated during the final stage of sulfide-saturated differentiation are lower than those observed, even using a minimum D_{Cu} value of 400 for sulfide (Ripley et al., 2002). Using a variable $\Delta^{57}Fe_{melt\text{-}solid}$ value (labeled variable α in Fig. 5a–c) does not change this result.

To explore whether the high Cu contents of the most evolved melts relative to model predictions could reflect contamination by cumulates derived from earlier fractionation episodes, 89:11 mixtures (the mixing ratio was chosen to bracket the range of evolved Anatahan lavas) between melt increments formed in the presence of residual sulfide and the aggregate cumulate formed immediately before the main phase of sulfide segregation (at F = 0.65) were calculated. The locus of these mixtures is shown as a separate melting curve on Fig. 5e; equivalent curves for V and Cr are shown on Fig. 5a and c. These model curves illustrate that contamination by small amounts of cumulate material can significantly increase melt Cu content, without substantially altering Cr and V contents and that this may be a viable explanation for the difference observed between modeled and melt Cu concentrations.

5.4. Implications for SO_2 degassing and the oxidation state of Anatahan lavas

Sulfur speciation and saturation in melts is a function of oxygen fugacity and melt composition, specifically Fe content. Melts with high fO_2, and thus where S is dissolved in the silicate melt predominantly as SO_4^{2-} typically have very high concentrations of S before sulfide-saturation (1500–4500 ppm; Luhr et al., 1984; Jugo, 2009). Melts with low fO_2, and thus where S is dissolved in the silicate melt as S^{2-} reach saturatation with a separate sulfide phase at moderate S contents (e.g., 1000–1400 ppm S, dependent on melt FeO_{tot} contents; Mavrogenes and O'Neill, 1999). The Cu contents (~100–170 ppm) of the more primitive, pre-magnetite-in (>4.2 wt% MgO, <51 wt% SiO_2) Anatahan and CIP arc magmas overlap with those of primitive Mar-

iana arc melts (100–114 ppm; Jenner, 2017) and both are high relative to MORB (60–70 ppm; Lee et al., 2012). These high Cu contents could imply that these more magnesian melts were initially sulfur-undersaturated and thus oxidized (Jugo et al., 2010) relative to MORB (c.f. Lee et al., 2012). However, if this were the case melt Cu contents should increase sharply as MgO decreases until the point sulfide appears on the liquidus. Instead, Anatahan and CIP magma Cu contents remain high and relatively constant until ~3.5 wt% MgO where they begin to decrease. This lends support to a scenario where melts are initially buffered with respect to sulfide before the appearance of magnetite on the liquidus which results in extensive sulfur saturation and removal. This scenario requires that the the melt is stored at pressures higher than those where S begins to partition into a separate vapor phase and degasses (i.e., >100 bar; Burgisser and Degruyter, 2015). In support of this scenario, olivine-hosted melt inclusions from Anatahan display moderately high and constant S contents of ~1100 ppm at ~4 wt% MgO, suggesting that S is not significantly lost during magmatic degassing during early differentiation (Shaw et al., 2008). A reduced role for SO_2 degassing also implies that the magmas underwent differentiation at relatively high pressures (>~100 bar). As SO_2 degassing can serve to decrease melt oxidation state (Anderson and Wright, 1972; Kelley and Cottrell, 2012; Moussallam et al., 2014) a reduced role for SO_2 degassing in the Anatahan suite implies that these magmas remained oxidized during differentiation until sufficient quantities of ferric iron had accumulated in the melt to trigger magnetite fractionation and the subsequent reduction of sulfate dissolved in the melt to sulfide.

Finally, the observed increase in Anatahan melt δ^{57}Fe with decreasing Cu (Fig. 5e) in the final stages of differentiation supports models in which Cu (and presumably other chalcophile elements) are sequestered by late sulfide saturation in initially oxidized, S-undersaturated melts (Jenner et al., 2010, 2012). This process provides an alternative means of sequestering these elements, which can also be removed by late-stage vapor/brine phase transport (Sun et al., 2015).

5.5. Co-variation of Fe with Tl, Mo, and V stable isotopes in the Marianas

The same sample powders analysed in this study have also been analysed for other heavy stable isotope systems. Here we explore insights gained from combining stable isotope systematics.

5.5.1. Thallium stable isotopes

Thallium has two stable isotopes, ^{203}Tl and ^{205}Tl. Thallium isotopes are unaffected by magmatic fractionation and are extremely sensitive to small additions of sedimentary materials to the source regions of arc melts (Prytulak et al., 2013, 2017a; Nielsen et al., 2016). Stable thallium isotopes have been measured on both the CIP lavas (Prytulak et al., 2013) and the Anatahan differentiation sequence (Prytulak et al., 2017a). No systematic relationships between Fe isotopes and Tl isotopes are present, although it is interesting that that sample GUG13, which bears the heaviest Fe isotope composition, and lowest Cu concentration (in Guguan) is also a significant outlier in terms of its Tl isotope composition. Prytulak et al. (2013) interpreted the Tl isotope signature of this sample in terms of the loss of light Tl during volcanic degassing, however, Fe is considerably less volatile than Tl. Moreover, the sample AGR19-02, which has demonstrably experienced magmatic degassing and loss of sulfur (Kelley and Cottrell, 2012), does not display highly fractionated bulk rock or mineral separate (magnetite and clinopyroxene) Fe isotope compositions. Other possible explanations for the heavy Fe isotope composition of sample GUG13 include the exsolution of isotopically light Fe-Cl fluids during differentiation (Heimann et al., 2008) or the accumulation of an isotopically heavy phase, although there is no petrographic evidence for the latter. Incorporation of hydrothermally altered oceanic crust lithologies is a possibility, as highly positive δ^{57}Fe values (up to +2.3‰) for some highly altered basalts have been documented and interpreted in terms of the preferential leaching and removal of isotopically light Fe (Rouxel et al., 2003). However, assimilation of hydrothermally-altered material would be expected to alter the oxygen isotope composition of affected samples and GUG13 has a mantle-like δ^{18}O value (Eiler et al., 2000).

Of the CVZ, Guguan displays some of the highest melt inclusion water contents, $Fe^{3+}/\Sigma Fe$ and Ba/La ratios (Kelley and Cottrell, 2009; Brounce et al., 2014). An alternative explanation for the heavy Fe isotope composition of GUG13 and the other Guguan samples could thus be an increase in $\Delta^{57}Fe_{melt\text{-}min}$ values, as a function of increased melt $Fe^{3+}/\Sigma Fe$ (Dauphas et al., 2014). However, more work is required to constrain the sensitivity of Fe isotope partitioning to melt composition, including the effects of melt $Fe^{3+}/\Sigma Fe$ and dissolved volatiles.

5.5.2. Molybdenum stable isotopes

There is active debate as to the cause of Mo stable isotope variations in igneous rocks (e.g., Willbold and Elliott, 2017); in particular whether magmatic differentiation can induce fractionation (Voegelin et al., 2014) or if fluid addition is more important (Freymuth et al., 2015). Samples with both Fe and Mo stable isotopes only encompass the CIP and no systematic relationships between Fe and Mo isotopes are observed. Molybdenum isotope data is not presently available for the differentiation sequence at Anatahan. Combination of Fe-Mo isotope systematics of such a sequence may yet shed light on the debate over Mo isotope fractionation during differentiation.

5.5.3. Vanadium stable isotopes

Vanadium has two stable isotopes, with variations reported as δ^{51}V (Nielsen et al., 2011; Prytulak et al., 2011). Similarly to iron, vanadium has multiple valence states and its elemental systematics have been employed as potential redox proxies (Canil, 1997; Canil, 2002; Lee et al., 2005). All of the CIP Fe samples in this study were obtained from aliquots of the digestions used for V isotopes (Prytulak et al., 2017b). Further Fe isotope analyses of the Anatahan differentiation sequence were made from the

same powders and in most cases the same dissolution as used for V isotopes (Prytulak et al., 2017b). Given their similar elemental characteristics, combined Fe-V stable isotope systematics may be of great value. Indeed, this is the first Fe-V stable isotope dataset to be interrogated.

We have argued here for a strong influence of magmatic differentiation and late sulfide saturation on the Fe isotopic compositions of the final erupted lavas/tephras in the Mariana arc, which is suggested to also influence the V isotope signatures of arc lavas/tephras (Prytulak et al., 2017b). There is little variation in the V isotopic composition of CIP lavas/tephras (Fig. 6a). In the case of Anatahan lavas, however, Prytulak et al. (2017b) observed that there are large variations in the V isotope composition, and this variation correlates with increasing indices of differentiation (e.g., MgO; Prytulak et al., 2017b), as the result of the removal of isotopically light V into magnetite during fractional crystallization. Despite the chemical similarities of Fe and V (i.e., that they can be multi-valent in silicate melts at fO_2 conditions relevant for terrestrial magmatism), their isotope systematics are partially decoupled during magmatic differentiation recorded in the Anatahan suite, as evident from the three trajectories shown in Fig. 6b. This can be simply understood in that Fe is concentrated in most major fractionating phases (olivine, pyroxene, oxides, molten and crystalline sulfide) whilst vanadium is a minor element and its isotope systematics in arc magmas are driven by magnetite fractionation alone.

Initially, crystallisation of olivine and (clino)pyroxene ± spinel will remove isotopically light Fe from the melt with a proportionally smaller effect on V isotopes (Fig. 6b; Group 1). The removal of significant quantities of magnetite then serves to decrease melt δ^{57}Fe and increase δ^{51}V (Group 2). Further differentiation serves to increase δ^{57}Fe as sulfide is removed from the melt (Group 3) and this increase in δ^{57}Fe is coupled to an increase in δ^{51}V of ~1.5‰ (Prytulak et al., 2017b), which provides evidence for the presence of both magnetite and sulfide on the liquidus at this stage, as V does not partition significantly into sulfide. The more muted increase in δ^{57}Fe can thus be interpreted in terms of the competing effects of magnetite (i.e. removal of isotopically heavy Fe) and sulfide (removal of isotopically light Fe) from the melt, and provide support for the presence of both magnetite and sulfide on the liquidus during differentiation. It is noteworthy that GUG13 is unremarkable in terms of its stable V isotope composition, but has a markedly lower Cu concentration (Fig. 3f) as well as isotopically heavy δ^{57}Fe, which would be compatible with sulfide removal.

This first combined Fe-V dataset shows the promise of a multi-isotope approach to distinguish between different fractionating assemblages and gain deeper insight into magmatic processes necessary to understand processes such as volcanic degassing, economic concentration of metals and the extent of magmatic fractionation versus magma mixing and assimilation. Critically, Fig. 6 clearly demonstrates that transition metal isotopes can be significantly altered during shallow-level differentiation processes and should not be used as direct proxies for the fO_2 of the source regions of magmas globally without careful consideration of the processes that we have discussed here (Figs. 5 and 6).

6. CONCLUSIONS

We have measured the Fe isotopic compositions of well characterized samples from the CIP of the Mariana arc. Iron isotopes do not record slab fluid or sediment melt contributions to the source region of Mariana arc magmas. Instead, the Fe isotope composition of these lavas predominantly reflect magmatic differentiation processes coupled with the previous melt extraction history of the source, although minor isotopic partitioning effects, due to variable melt Fe^{3+}/Fe_{tot} or water content cannot be ruled out. As noted in earlier studies (Williams et al., 2004, 2005; Nebel et al., 2013, 2015), melt extraction has the potential to generate arc magma mantle source regions with Fe isotope compositions lighter than primitive mantle. This potential variation in source region Fe isotope composition, coupled with isotopic fractionation induced by magmatic differentiation, means that variations in magmatic δ^{57}Fe (e.g. between arc basalts and MORB) cannot be used to infer differences in melt oxygen fugacity without this contextual information (Dauphas et al., 2009).

Substantial Fe isotope variation is observed within the Anatahan basaltic-andesite to dacite differentiation sequence. These isotopic variations, coupled with decreasing Cr, V and Cu concentrations, can be linked to three closed–system differentiation stages (and magmatic groups): (i) olivine and (clino-)pyroxene ± spinel fractionation; (ii) the onset of magnetite and minor sulfide fractionation, where sulfide saturation is triggered by the appearance of magnetite on the liquidus; (iii) extensive magnetite and molten or crystalline sulfide fractionation. The negative co-variation between Fe isotopes and Cu contents in the most differentiated samples provides evidence for the removal of Cu into molten or crystalline sulfide phases, which has implications for Cu porphyry formation. This fractionation sequence also provides a means of generating evolved melts with isotopically heavy Fe isotope compositions that must (according to mass balance) coexist with isotopically light cumulates which has implications for the Fe isotope composition of the continental crust.

Iron and vanadium stable isotopes can be used together in closed-system differentiated magma suites to build a picture of silicate, oxide and sulfide phase fractionation. The combined Fe and V isotope systematics also demonstrate that the transition metal stable isotope signatures of magmatic rocks cannot be used as direct redox proxies without constraining the impact of magmatic differentiation and partial melting processes on these systems.

ACKNOWLEDGEMENTS

We are extremely grateful to Tim Elliott for providing samples, Geoff Nowell for his help in making isotope ratio measurements, Paolo Sossi, Oliver Nebel, Lois Salem and Frances Jenner for insightful comments and suggestions about data presentation, and John Foden, for sharing his unpublished data. We also thank Oliver Nebel, Cin-Ty Lee and an anonymous reviewer for their very helpful and constructive comments. Stefan Weyer and Marc

Norman are also thanked for their suggestions and editorial handling. HMW acknowledges an ERC Starting Grant (“HabitableP lanet”, 306655) and NERC “Deep Volatiles” (NE/M0003/1) and “Tellurium and Selenium Cycling and Supply” (NE/M010848/1) Consortia Grants. JP acknowledges funding from NERC fellowship NE/H01313X/2.

APPENDIX A. SUPPLEMENTARY MATERIAL

Supplementary data associated with this article can be found, in the online version, at https://doi.org/10.1016/j.gca.2018.02.008.

REFERENCES

Adam J. and Green T. (2006) Trace element partitioning between mica-and amphibole-bearing garnet lherzolite and hydrous basanitic melt: 1. Experimental results and the investigation of controls on partitioning behaviour. *Contrib. Mineral. Petrol.* **152**, 1–17.

Anderson A. T. and Wright T. L. (1972) Phenocrysts and glass inclusions and their bearing on oxidation and mixing of basaltic magmas, Kilauea volcano, Hawaii. *Am. Mineral.* **57**(1-2), 188.

Arculus R. J. (1994) Aspects of magma genesis in arcs. *Lithos* **33**, 189–208.

Avanzinelli R., Prytulak J., Skora S., Heumann A., Koetsier G. and Elliott T. (2012) Combined U-238-Th-230 and U-235-Pa-231 constraints on the transport of slab-derived material beneath the Mariana Islands. *Geochim. Cosmochim. Acta* **92**, 308–328.

Beard B. L., Johnson C. M., Skulan J. L., Nealson K. H., Cox L. and Sun H. (2003) Application of Fe isotopes to tracing the geochemical and biological cycling of Fe. *Chem. Geol.* **195**, 87–117.

Bloomer S. H., Stern R. J., Fisk E. and Geschwind C. H. (1989) Shoshonitic volcanism in the northern Mariana Arc. 1. Mineralogic and major and trace-element characteristics. *J. Geophys. Res.-Solid Earth Planets* **94**, 4469–4496.

Botcharnikov R. E., Almeev R. R., Koepke J. and Holtz F. (2008) Phase relations and liquid lines of descent in hydrous ferrobasalt – implications for the Skaergaard intrusion and Columbia River flood basalts. *J. Petrol.* **49**, 1687–1727.

Brounce M. N., Kelley K. A. and Cottrell E. (2014) Variations in $Fe^{3+}/\Sigma Fe$ of Mariana Arc basalts and mantle wedge fO(2). *J. Petrol.* **55**, 2513–2536.

Burgisser A. and Degruyter W. (2015) Magma ascent and degassing at shallow levels. In *The Encyclopedia of Volcanoes* (eds. H. Sigurdsson, B. Houghton, S. McNutt, H. Rymer and J. Stix), second ed. Elsevier, pp. 225–236. https://doi.org/10.1016/B978-0-12-385938-9.00011-0.

Canil D. (1997) Vanadium partitioning and the oxidation state of Archaean komatiite magmas. *Nature* **389**, 842–845.

Canil D. (2002) Vanadium in peridotites, mantle redox and tectonic environments: Archean to present. *Earth Planet. Sci. Lett.* **195**, 75–90.

Carmichael I. S. E. (1991) The redox states of basic and silicic magmas – a reflection of their source regions. *Contrib. Mineral. Petrol.* **106**, 129–141.

Dauphas N., Craddock P. R., Asimow P. D., Bennett V. C., Nutman A. P. and Ohnenstetter D. (2009) Iron isotopes may reveal the redox conditions of mantle melting from Archean to Present. *Earth Planet. Sci. Lett.* **288**, 255–267.

Dauphas N., Roskosz M., Alp E., Neuville D., Hu M., Sio C., Tissot F., Zhao J., Tissandier L., Médard E. and Cordier C. (2014) Magma redox and structural controls on iron isotope variations in Earth’s mantle and crust. *Earth Planet. Sci. Lett.* **398**, 127–140.

Dauphas N., John S. and Rouxel O. (2017) Iron isotope systematics. *Rev. Mineral. Geochem.* **82**, 415–510.

Debret B., Millet M.-A., Pons M.-L., Bouilhol P., Inglis E. and Williams H. M. (2016) Isotopic evidence for iron mobility during subduction. *Geology* **44**(3), 215–218.

de Moor J. M., Fischer T. P., Hilton D. R., Hauri E., Jaffe L. A. and Camacho J. T. (2005) Degassing at Anatahan volcano during the May 2003 eruption: implications from petrology, ash leachates, and SO_2 emissions. *J. Volcanol. Geoth. Res.* **146**, 117–138.

Dixon J. E., Stolper E. M. and Holloway J. R. (1995) An experimental study of water and carbon dioxide solubilities in mid-ocean ridge basaltic liquids. Part I. Calibration and solubility models. *J. Petrol.* **36**, 1607–1630.

Eiler J. M., Crawford A., Elliott T., Farley K. A., Valley J. W. and Stolper E. M. (2000) Oxygen isotope geochemistry of oceanic-arc lavas. *J. Petrol.* **41**, 229–256.

Elliott T., Plank T., Zindler A., White W. and Bourdon B. (1997) Element transport from slab to volcanic front at the Mariana arc. *J. Geophys. Res. – Solid Earth* **102**, 14991–15019.

Freymuth H., Vils F., Willbold M., Taylor R. N. and Elliott T. (2015) Molybdenum mobility and isotopic fractionation during subduction at the Mariana arc. *Earth Planet. Sci. Lett.* **432**, 176–186.

Frost D. J. and McCammon C. A. (2008) The redox state of Earth’s mantle. *Annu. Rev. Earth Planet. Sci.* **36**, 389–420.

Gaetani G. A. and Grove T. L. (1997) Partitioning of moderately siderophile elements among olivine, silicate melt, and sulfide melt: constraints on core formation in the Earth and Mars. *Geochim. Cosmochim. Acta* **61**, 1829–1846.

Hamilton D., Burnham C. W. and Osborn E. (1964) The solubility of water and effects of oxygen fugacity and water content on crystallization in mafic magmas. *J. Petrol.* **5**, 21–39.

Hedenquist J. W. and Lowenstern J. B. (1994) The role of magmas in the formation of hydrothermal ore-deposits. *Nature* **370**, 519–527.

Heimann A., Beard B. L. and Johnson C. M. (2008) The role of volatile exsolution and sub-solidus fluid/rock interactions in producing high Fe-56/Fe-54 ratios in siliceous igneous rocks. *Geochim. Cosmochim. Acta* **72**, 4379–4396.

Hibbert K., Williams H. M., Kerr A. C. and Puchtel I. (2012) Iron isotopes in ancient and modern komatiites: evidence for a uniformly oxidised mantle from the Archean to present. *Earth Planet. Sci. Lett.* **321**, 198–207.

Jayasuriya K. D., O’Neill H. S., Berry A. J. and Campbell S. J. (2004) A Mossbauer study of the oxidation state of Fe in silicate melts. *Am. Mineral.* **89**, 1597–1609.

Jenner F. E., O’Neill H. S. C., Arculus R. J. and Mavrogenes J. A. (2010) The magnetite crisis in the evolution of arc-related magmas and the initial concentration of Au, Ag and Cu. *J. Petrol.* **51**, 2445–2464.

Jenner F. E., Arculus R. J., Mavrogenes J. A., Dyriw N. J., Nebel O. and Hauri E. H. (2012) Chalcophile element systematics in volcanic glasses from the northwestern Lau Basin. *Geochem. Geophys. Geosyst.* **13**.

Jenner F. E. (2017) Cumulate causes for the low contents of sulfide loving elements in the continental crust. *Sci. Nat. Geoscience* **10**, 524–529.

Jugo P. J. (2009) Sulfur content at sulfide saturation in oxidized magmas. *Geology* **37**(5), 415–418.

Jugo P. J., Wilke M. and Botcharnikov R. E. (2010) Sulfur K-edge XANES analysis of natural and synthetic basaltic glasses: implications for S speciation and S content as function of oxygen fugacity. *Geochim. Cosmochim. Acta* **74**, 5926–5938.

Kelley K. A. and Cottrell E. (2009) Water and the oxidation state of subduction zone magmas. *Science* **325**, 605–607.

Kelley K. A., Plank T., Newman S., Stolper E. M., Grove T. L., Parman S. and Hauri E. H. (2010) Mantle melting as a function of water content beneath the Mariana Arc. *J. Petrol.* **51**, 1711–1738.

Kelley K. A. and Cottrell E. (2012) The influence of magmatic differentiation on the oxidation state of Fe in a basaltic arc magma. *Earth Planet. Sci. Lett.* **329**, 109–121.

Kent A. J. R. and Elliott T. R. (2002) Melt inclusions from Marianas arc lavas: implications for the composition and formation of island arc magmas. *Chem. Geol.* **183**, 263–286.

Kitada K., Seama N., Yamazaki T., Nogi Y. and Suyehiro K. (2006) Distinct regional differences in crustal thickness along the axis of the Mariana Trough, inferred from gravity anomalies. *Geochem. Geophys. Geosyst.* **7**, Q04011. https://doi.org/10.1029/2005GC001119.

Konter J. G., Pietruszka A. J., Hanan B. B., Finlayson V. A., Craddock P. R., Jackson M. G. and Dauphas N. (2016) Unusual delta Fe-56 values in Samoan rejuvenated lavas generated in the mantle. *Earth Planet. Sci. Lett.* **450**, 221–232.

Lee C. T. A., Leeman W. P., Canil D. and Li Z. X. A. (2005) Similar V/Sc systematics in MORB and arc basalts: implications for the oxygen fugacities of their mantle source regions. *J. Petrol.* **46**, 2313–2336.

Lee C.-T. A., Luffi P., Chin E. J., Bouchet R., Dasgupta R., Morton D. M., Le Roux V., Yin Q.-Z. and Jin D. (2012) Copper systematics in arc magmas and implications for crust-mantle differentiation. *Science* **336**, 64–68.

Liu X., Xiong X., Audetat A., Li Y., Song M., Li L., Sun W. and Ding X. (2014) Partitioning of copper between olivine, orthopyroxene, clinopyroxene, spinel, garnet and silicate melts at upper mantle conditions. *Geochim. Cosmochim. Acta* **125**, 1–22.

Luhr J. F., Carmichael I. S. and Varekamp J. C. (1984) The 1982 eruptions of El Chichón Volcano, Chiapas, Mexico: mineralogy and petrology of the anhydritebearing pumices. *J. Volcanol. Geoth. Res.* **23**(1–2), 69–108.

Macris C. A., Manning C. E. and Young E. D. (2015) Crystal chemical constraints on inter-mineral Fe isotope fractionation and implications for Fe isotope disequilibrium in San Carlos mantle xenoliths. *Geochim. Cosmochim. Acta* **154**, 168–185.

Mallmann G. and O'Neill H. S. C. (2009) The crystal/melt partitioning of V during mantle melting as a function of oxygen fugacity compared with some other elements (Al, P, Ca, Sc, Ti, Cr, Fe, Ga, Y, Zr and Nb). *J. Petrol.* **50**, 1765–1794.

Martindale M., Skora S., Pickles J., Elliott T., Blundy J. and Avanzinelli R. (2013) High pressure phase relations of subducted volcaniclastic sediments from the west pacific and their implications for the geochemistry of Mariana arc magmas. *Chem. Geol.* **342**, 94–109.

Martınez F. and Taylor B. (2003) Controls on back-arc crustal accretion: Insights from the Lau, Manus and Mariana basins. In Intra-oceanic Subduction Systems: Tectonic and Magmatic Processes (eds. R. D. Larter and P. T. Leat). Geol. Soc. Spec. Publ., vol. 218. pp. 19–54.

Mavrogenes J. A. and O'Neill H. S. C. (1999) The relative effects of pressure, temperature and oxygen fugacity on the solubility of sulfide in mafic magmas. *Geochim. Cosmochim. Acta* **63**, 1173–1180.

Meijer A. and Reagan M. (1981) Petrology and geochemistry of the island of Sarigan in the Mariana Arc – calc-alkaline volcanism in an oceanic setting. *Contrib. Mineral. Petrol.* **77**, 337–354.

Moussallam Y., Oppenheimer C., Scaillet B., Gaillard F., Kyle P., Peters N., Hartley M., Berlo K. and Donovan A. (2014) Tracking the changing oxidation state of Erebus magmas, from mantle to surface, driven by magma ascent and degassing. *Earth Planet. Sci. Lett.* **393**, 200–209.

Mysen B. O. (1992) Iron and phosphorus in calcium silicate quenched melts. *Chem. Geol.* **98**, 175–202.

Nebel O., Arculus R. J., Sossi P. A., Jenner F. E. and Whan T. H. E. (2013) Iron isotopic evidence for convective resurfacing of recycled arc-front mantle beneath back-arc basins. *Geophys. Res. Lett.* **40**, 5849–5853.

Nebel O., Sossi P. A., Benard A., Wille M., Vroon P. Z. and Arculus R. J. (2015) Redox-variability and controls in subduction zones from an iron-isotope perspective. *Earth Planet. Sci. Lett.* **432**, 142–151.

Nielsen S. G., Prytulak J. and Halliday A. N. (2011) Determination of precise and accurate V-51/V-50 isotope ratios by MC-ICP-MS, Part 1: chemical separation of vanadium and mass spectrometric protocols. *Geostand. Geoanal. Res.* **35**, 293–306.

Nielsen S. G., Yogodzinski G., Prytulak J., Plank T., Kay S. M., Kay R. W., Blusztajn J., Owens J. D., Auro M. and Kading T. (2016) Tracking along-arc sediment inputs to the Aleutian arc using thallium isotopes. *Geochim. Cosmochim. Acta* **181**, 217–237.

O'Neill H. S. C. and Mavrogenes J. A. (2002) The sulfide capacity and the sulfur content at sulfide saturation of silicate melts at 1400 C and 1 bar. *J. Petrol.* **43**, 1049–1087.

Osborn E. F. (1959) Role of oxygen pressure in the crystallization and differentiation of basaltic magma. *Am. J. Sci.* **257**, 609–647.

Palme H. and O'Neill H. S. C. (2004) Cosmochemical estimates of mantle composition. In *Treatise on Geochemistry* (eds. H. D. Holland and K. K. Turrekian). Elsevier, Amsterdam, pp. 1–38.

Plank T. (2005) Constraints from thorium/lanthanum on sediment recycling at subduction zones and the evolution of the continents. *J. Petrol.* **46**, 921–944.

Plank T., Kelley K. A., Zimmer M. M., Hauri E. H. and Wallace P. J. (2013) Why do mafic arc magmas contain similar to 4 wt% water on average? *Earth Planet. Sci. Lett.* **364**, 168–179.

Poitrasson F. and Freydier R. (2005) Heavy iron isotope composition of granites determined by high resolution MC-ICP-MS. *Chem. Geol.* **222**, 132–147.

Polyakov V. B. and Mineev S. D. (2000) The use of Mössbauer spectroscopy in stable isotope geochemistry. *Geochim. Cosmochim. Acta* **64**, 849–865.

Polyakov V. B., Clayton R. N., Horita J. and Mineev S. D. (2007) Equilibrium iron isotope fractionation factors of minerals: reevaluation from the data of nuclear inelastic resonant X-ray scattering and Mossbauer spectroscopy. *Geochim. Cosmochim. Acta* **71**, 3833–3846.

Polyakov V. B. (2009) Equilibrium iron isotope fractionation at core-mantle boundary conditions. *Science* **323**, 912–914.

Prytulak J., Nielsen S. G. and Halliday A. N. (2011) Determination of precise and accurate V-51/V-50 isotope ratios by multi-collector ICP-MS, Part 2: Isotopic composition of six reference materials plus the allende chondrite and verification tests. *Geostand. Geoanal. Res.* **35**, 307–318.

Prytulak J., Nielsen S. G., Plank T., Barker M. and Elliott T. (2013) Assessing the utility of thallium and thallium isotopes for tracing subduction zone inputs to the Mariana arc. *Chem. Geol.* **345**, 139–149.

Prytulak J., Brett A., Webb M., Plank T., Rehkämper M., Savage P. and Woodhead J. (2017a) Thallium elemental behavior and stable isotope fractionation during magmatic processes. *Chem. Geol.* **448**, 71–83.

Prytulak J., Sossi P. A., Halliday A. N., Plank T., Savage P. S. and Woodhead J. D. (2017b) Stable vanadium isotopes as a redox proxy in magmatic systems? *Geochem. Perspect. Lett.* **3**, 75–84.

Ripley E. M., Brophy J. G. and Li C. S. (2002) Copper solubility in a basaltic melt and sulfide liquid/silicate melt partition coefficients of Cu and Fe. *Geochim. Cosmochim. Acta* **66**, 2791–2800.

Roskosz M., Sio C. K. I., Dauphas N., Bi W. L., Tissot F. L. H., Hu M. Y., Zhao J. Y. and Alp E. E. (2015) Spinel-olivine-pyroxene equilibrium iron isotopic fractionation and applications to natural peridotites. *Geochim. Cosmochim. Acta* **169**, 184–199.

Rouxel O., Dobbek N., Ludden J. and Fouquet Y. (2003) Iron isotope fractionation during oceanic crust alteration. *Chem. Geol.* **202**, 155–182.

Sandwell D. T. and Smith W. H. F. (1997) Marine gravity anomaly from Geosat and ERS 1 satellite altimetry. *J. Geophys. Res.* **102** (B5), 10039–10054.

Schmidt B. C., Holtz F. and Pichavant M. (1999) Water solubility in haplogranitic melts coexisting with H2O-H-2 fluids. *Contrib. Mineral. Petrol.* **136**, 213–224.

Schoenberg R., Marks M. A., Schuessler J. A., von Blanckenburg F. and Markl G. (2009) Fe isotope systematics of coexisting amphibole and pyroxene in the alkaline igneous rock suite of the Ilímaussaq Complex, South Greenland. *Chem. Geol.* **258**(1), 65–77.

Schuessler J. A., Schoenberg R., Behrens H. and Blanckenburg F. v. (2007) The experimental calibration of the iron isotope fractionation factor between pyrrhotite and peralkaline rhyolitic melt. *Geochim. Cosmochim. Acta* **71**, 417–433.

Schuessler J. A., Schoenberg R. and Sigmarsson O. (2009) Iron and lithium isotope systematics of the Hekla volcano, Iceland – evidence for Fe isotope fractionation during magma differentiation. *Chem. Geol.* **258**, 78–91.

Shahar A., Young E. D. and Manning C. E. (2008) Equilibrium high-temperature Fe isotope fractionation between fayalite and magnetite: an experimental calibration. *Earth Planet. Sci. Lett.* **268**, 330–338.

Shaw A. M., Hauri E. H., Fischer T. P., Hilton D. R. and Kelley K. A. (2008) Hydrogen isotopes in Mariana arc melt inclusions: implications for subduction dehydration and the deep-Earth water cycle. *Earth Planet. Sci. Lett.* **275**, 138–145.

Sisson T. W. and Grove T. L. (1993) Experimental investigations of the role of H2O in calc-alkaline differentiation and subduction zone magmatism. *Contrib. Mineral. Petrol.* **113**, 143–166.

Sossi P. A., Foden J. D. and Halverson G. P. (2012) Redox-controlled iron isotope fractionation during magmatic differentiation: an example from the Red Hill intrusion, S. Tasmania. *Contrib. Mineral. Petrol.* **164**, 757–772.

Sossi P. A., Nebel O. and Foden J. (2016) Iron isotope systematics in planetary reservoirs. *Earth Planet. Sci. Lett.* **452**, 295–308.

Stern R. J. and Ito E. (1983) Trace-element and isotopic constraints on the source of magmas in the active Volcano and Mariana island arcs, Western Pacific. *J. Volcanol. Geoth. Res.* **18**, 461–482.

Straub S. M. and Layne G. D. (2003) The systematics of chlorine, fluorine, and water in Izu arc front volcanic rocks: implications for volatile recycling in subduction zones. *Geochim. Cosmochim. Acta* **67**, 4179–4203.

Sun W., Huang R.-F., Li H., Hu Y.-B., Zhang C.-C., Sun S.-J., Zhang L.-P., Ding X., Li C.-Y., Zartman R. E. and Ling M.-X. (2015) Porphyry deposits and oxidized magmas. *Ore Geol. Rev.* **65, Part1**, 97–131.

Teng F. Z., Dauphas N. and Helz R. T. (2008) Iron isotope fractionation during magmatic differentiation in Kilauea Iki Lava Lake. *Science* **320**, 1620–1622.

Teng F.-Z., Dauphas N., Huang S. and Marty B. (2013) Iron isotopic systematics of oceanic basalts. *Geochim. Cosmochim. Acta* **107**, 12–26.

Toplis M. J., Dingwell D. B. and Libourel G. (1994) The effect of phosphorus on the iron redox ratio, viscosity, and density of an evolved ferro-basalt. *Contrib. Mineral. Petrol.* **117**, 293–304.

Toplis M. J. and Carroll M. R. (1995) An experimental-study of the influence of oxygen fugacity on Fe-Ti oxide stability, phase-relations, and mineral-melt equilibria in ferro-basaltic systems. *J. Petrol.* **36**, 1137–1170.

Toplis M. J. and Carroll M. R. (1996) Differentiation of ferro-basaltic magmas under conditions open and closed to oxygen: implications for the Skaergaard intrusion and other natural systems. *J. Petrol.* **37**, 837–858.

Toplis M. J. and Corgne A. (2002) An experimental study of element partitioning between magnetite, clinopyroxene and iron-bearing silicate liquids with particular emphasis on vanadium. *Contrib. Mineral. Petrol.* **144**, 22–37.

Voegelin A. R., Pettke T., Greber N. D., von Niederhausern B. and Nagler T. F. (2014) Magma differentiation fractionates Mo isotope ratios: evidence from the Kos Plateau Tuff (Aegean Arc). *Lithos* **190**, 440–448.

Wade J. A., Plank T., Stern R. J., Tollstrup D. L., Gill J. B., O'Leary J. C., Eiler J. M., Moore R. B., Woodhead J. D., Trusdell F., Fischer T. P. and Hilton D. R. (2005) The May 2003 eruption of Anatahan volcano, Mariana Islands: geochemical evolution of a silicic island-arc volcano. *J. Volcanol. Geoth. Res.* **146**, 139–170.

Wade J. A., Plank T., Hauri E. H., Kelley K. A., Roggensack K. and Zimmer M. (2008) Prediction of magmatic water contents via measurement of H2O in clinopyroxene phenocrysts. *Geology* **36**, 799–802.

Waters L. E. and Lange R. A. (2016) No effect of H2O degassing on the oxidation state of magmatic liquids. *Earth Planet. Sci. Lett.* **447**, 48–59.

Weyer S., Anbar A. D., Brey G. P., Munker C., Mezger K. and Woodland A. B. (2005) Iron isotope fractionation during planetary differentiation. *Earth Planet. Sci. Lett.* **240**, 251–264.

Weyer S. and Ionov D. A. (2007) Partial melting and melt percolation in the mantle: the message from Fe isotopes. *Earth Planet. Sci. Lett.* **259**, 119–133.

Wilkinson J. J. (2013) Triggers for the formation of porphyry ore deposits in magmatic arcs. *Nat. Geosci.* **6**, 917–925.

Willbold M. and Elliott T. (2017) Molybdenum isotope variations in magmatic rocks. *Chem. Geol.*.

Williams H. M., McCammon C. A., Peslier A. H., Halliday A. N., Teutsch N., Levasseur S. and Burg J. P. (2004) Iron isotope fractionation and the oxygen fugacity of the mantle. *Science* **304**, 1656–1659.

Williams H. M., Peslier A. H., McCammon C., Halliday A. N., Levasseur S., Teutsch N. and Burg J. P. (2005) Systematic iron isotope variations in mantle rocks and minerals: the effects of partial melting and oxygen fugacity. *Earth Planet. Sci. Lett.* **235**, 435–452.

Williams H. M. and Bizimis M. (2014) Iron isotope tracing of mantle heterogeneity within the source regions of oceanic basalts. *Earth Planet. Sci. Lett.* **404**, 396–407.

Woodhead J. D. and Fraser D. G. (1985) Pb, Sr and Be-10 isotopic studies of volcanic-rocks from the Northern Mariana Islands – implications for magma genesis and crustal recycling in the Western Pacific. *Geochim. Cosmochim. Acta* **49**, 1925–1930.

Woodhead J. D. (1988) The origin of geochemical variations in Mariana lavas – a general model for petrogenesis in intra-oceanic island arcs. *J. Petrol.* **29**, 805–830.

Woodhead J. D. (1989) Geochemistry of the Mariana Arc (Western Pacific) – source composition and processes. *Chem. Geol.* **76**, 1–24.

Woodhead J., Eggins S. and Gamble J. (1993) High-field strength and transition element systematics in island-arc and back-arc basin basalts – evidence for multiphase melt extraction and a depleted mantle wedge. *Earth Planet. Sci. Lett.* **114**, 491–504.

Woodhead J. D., Hergt J. M., Davidson J. P. and Eggins S. M. (2001) Hafnium isotope evidence for 'conservative' element mobility during subduction zone processes. *Earth Planet. Sci. Lett.* **192**, 331–346.

Woodland A. B. and Koch M. (2003) Variation in oxygen fugacity with depth in the upper mantle beneath the Kaapvaal craton, Southern Africa. *Earth Planet. Sci. Lett.* **214**, 295–310.

Young E. D., Manning C. E., Schauble E. A., Shahar A., Macris C. A., Lazar C. and Jordan M. (2015) High-temperature equilibrium isotope fractionation of non-traditional stable isotopes: experiments, theory, and applications. *Chem. Geol.* **395**, 176–195.

Zimmer M. M., Plank T., Hauri E. H., Yogodzinski G. M., Stelling P., Larsen J., Singer B., Jicha B., Mandeville C. and Nye C. J. (2010) The role of water in generating the calc-alkaline trend: new volatile data for aleutian magmas and a new tholeiitic index. *J. Petrol.* **51**, 2411–2444.

Associate editor: Stefan Weyer